Polyhydroxyalkylations for alkali-stable cationic polymers as hydroxide exchange membranes

Pan, Dong

2023

Document Version:
Publisher's PDF, also known as Version of record

Polyhydroxyalkylations for alkali-stable cationic polymers as hydroxide exchange membranes

DONG PAN | CENTRE FOR ANALYSIS AND SYNTHESIS | LUND UNIVERSITY

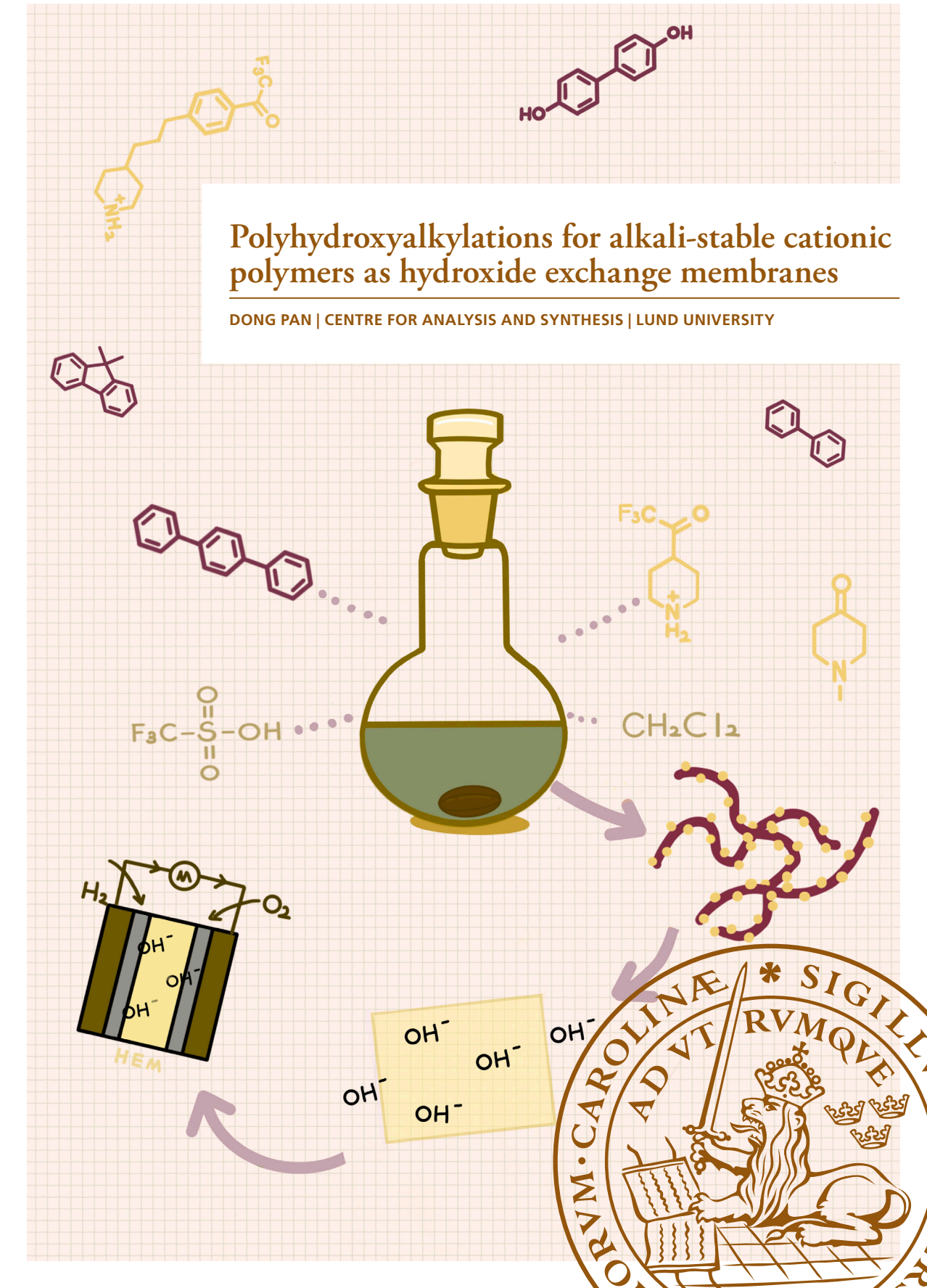

Polyhydroxyalkylations for alkali-stable cationic polymers as hydroxide exchange membranes

Polyhydroxyalkylations for alkali-stable cationic polymers as hydroxide exchange membranes

Dong Pan

LUND
UNIVERSITY

DOCTORAL DISSERTATION

by due permission of the Faculty of Engineering, Lund University, Sweden.

To be defended at Kemicentrum, Lecture Hall K:A on April 21, at 13:00.

Faculty opponent
Dr. Cristina Iojoiu,
Université Grenoble-Alpes, Grenoble Institute of Technology

Organization LUND UNIVERSITY	**Document name** Doctoral Dissertation
	Date of issue 2023-04-21
Author(s) Dong Pan	Sponsoring organization

Title and subtitle
Polyhydroxyalkylations for alkali-stable cationic polymers as hydroxide exchange membranes

Abstract

To alleviate worldwide dependence on fossil fuels for energy production and considerably reduce CO_2 emissions, green energy sources and sustainable energy solutions are in high demand. Fuel cells are environmental-friendly electrochemical devices which may use clean fuels, e.g., green hydrogen gas, to generate electricity. Meanwhile, water electrolyzers provide an efficient strategy to produce green hydrogen without emitting greenhouse gases. Research on fuel cells and electrolyzers, especially on the component level, is currently progressing rapidly. Applying a solid electrolyte instead of liquid one potentially simplifies the cell operation and has motivated intensive research on suitable ion-conductive polymer electrolytes. Ion exchange membranes are fabricated from polymers functionalized with ionic groups. To date, devices employing proton exchange membranes (PEMs) are already commercialized, or on the brink of broad commercialization, but are rather expensive because of the requirement to use noble metal catalysts under acidic conditions. Shifting to alkaline operating conditions allows the potential use of non-platinum-group catalysts, e.g., silver or nickel, making the alkaline devices cost-effective alternatives. Still, these devices cannot fully compete with the PEM-based ones yet because the components such as the required hydroxide exchange membrane (HEM) do not yet have the necessary performance and durability.

At present, two major issues with the HEMs are their insufficient lifetime and conductivity, which closely affect the life span and power output of the devices. The aim of the present thesis work was to prepare HEMs with high chemical stability and hydroxide conductivity. Using superacid-mediated polyhydroxyalkylation reactions, several series of different aromatic polymers functionalized with alkali-stable cations were synthesized and studied. HEMs were prepared from the polymers, and investigated in terms of water uptake, morphology, ion conductivity, thermal stability, and with a special emphasis on the alkaline stability. Changes of the HEMs' molecular structure from chemical degradation after severe alkaline treatments were carefully studied and the degradation mechanisms were elucidated.

Overall, most of the studied HEMs reached high hydroxide conductivities, approaching 180 mS cm^{-1} at 80 °C. To enhance the high alkaline stability of the HEMs, different strategies to vary the polymer/cation arrangements were employed. The combined results especially showed that attaching the cations to a rigid polymer backbone *via* flexible spacer units is highly beneficial to protect the HEM from hydroxide ion attack.

Key words quaternary ammoniums, aromatic polymers, chemical resistance, ion conductivity

Classification system and/or index terms (if any)

Supplementary bibliographical information	**Language** English
ISSN and key title	**ISBN** 978-91-7422-934-9 (Print) 978-91-7422-935-6 (Digital)
Recipient's notes	**Number of pages** 188 Price
	Security classification

Signature Dong Pan Date 2023-03-06

Polyhydroxyalkylations for alkali-stable cationic polymers as hydroxide exchange membranes

Dong Pan

LUND
UNIVERSITY

Cover photo (front): illustration a polyhydroxyalkylation reaction flask, reactants, cationic polymers, a hydroxide exchange membrane (HEM), and an HEM fuel cell, by Dong Pan.

Cover photo (back): photograph of the Lund University main building, by Kennet Ruona (from LU image and media bank).

Faculty of Engineering
Department of Chemistry, CAS

ISBN 978-91-7422-934-9 (print)
ISBN 978-91-7422-935-6 (digital)

Printed in Sweden by Media-Tryck, Lund University
Lund 2023

Abstract

To alleviate worldwide dependence on fossil fuels for energy production and considerably reduce CO_2 emissions, green energy sources and sustainable energy solutions are in high demand. Fuel cells are environmental-friendly electrochemical devices which may use clean fuels, e.g., green hydrogen gas, to generate electricity. Meanwhile, water electrolyzers provide an efficient strategy to produce green hydrogen without emitting greenhouse gases. Research on fuel cells and electrolyzers, especially on the component level, is currently progressing rapidly. Applying a solid electrolyte instead of liquid one potentially simplifies the cell operation and has motivated intensive research on suitable ion-conductive polymer electrolytes. Ion exchange membranes are fabricated from polymers functionalized with ionic groups. To date, devices employing proton exchange membranes (PEMs) are already commercialized, or on the brink of broad commercialization, but are rather expensive because of the requirement to use noble metal catalysts under acidic conditions. Shifting to alkaline operating conditions allows the potential use of non-platinum-group catalysts, e.g., silver or nickel, making the alkaline devices cost-effective alternatives. Still, these devices cannot fully compete with the PEM-based ones yet because the components such as the required hydroxide exchange membrane (HEM) do not yet have the necessary performance and durability.

At present, two major issues with the HEMs are their insufficient lifetime and conductivity, which closely affect the life span and power output of the devices. The aim of the present thesis work was to prepare HEMs with high chemical stability and hydroxide conductivity. Using superacid-mediated polyhydroxyalkylation reactions, several series of different aromatic polymers functionalized with alkali-stable cations were synthesized and studied. HEMs were prepared from the polymers, and investigated in terms of water uptake, morphology, ion conductivity, thermal stability, and with a special emphasis on the alkaline stability. Changes of the HEMs' molecular structure from chemical degradation after severe alkaline treatments were carefully studied and the degradation mechanisms were elucidated.

Overall, most of the studied HEMs reached high hydroxide conductivities, approaching 180 mS cm^{-1} at 80 °C. To enhance the high alkaline stability of the HEMs, different strategies to vary the polymer/cation arrangements were employed. The combined results especially showed that attaching the cations to a rigid polymer backbone *via* flexible spacer units is highly beneficial to protect the HEM from hydroxide ion attack.

Table of contents

Acknowledgments

It has been the best four and a half years of my life being a doctoral student with continuous support and encouragement around. My deepest gratitude goes to my supervisor **Patric**, for offering me the position and everything else that comes with it. Your calm and optimistic attitude toward research has influenced me to a great extent. I will always be grateful that you have guided me growing up as a researcher.

I would like to thank my co-supervisor **Bao**, previous and present department representatives, **Lotta** and **Kenneth**, for giving valuable advice about my research and studies. I want to thank **Maria**, **Sara**, **Katarina**, and **Kornelije**, who have been kindly helping with administrative affairs, chemical orders, and maintenance of instruments, making research life much simpler. Also, thanks to everyone at Polymat and CAS for creating a friendly and welcoming working environment.

I have worked closely with fantastic colleagues in the polymer electrolyte sub-group, who enriched my work life and made every day memorable. They are not only knowledgeable but also have been very patient with my questions. **Joel**, my go-to person from day one, thank you for all the enjoyable teaching & learning moments of research and life. It wouldn't have been as fun if it wasn't for you. **Huong**, thank you for generously sharing your research experience, which has saved me loads of time and struggles in the projects. **Hannes**, thank you for being a reliable person to keep the labs whole. Your rigorous principle and funny jokes are very much appreciated. **Andrit**, I am thankful to have you present at many highs and lows in daily research. Thank you for always being in the office or lab to listen and try to help. **Si**, thank you for the fruitful teamwork, supplying Si's monomer, being a great lunch buddy, and being extremely helpful whenever I am struggling with my words.

Workwise, I have received help from other members in the group. This thesis contains important input from them in many ways. Thank you, **Choi**, **Haiyue**, **Nitin**, **Oskar**, **Olivier**, **Pegah**, **Triet**, **Anuja**, **Isabell**, **Niklas**, **Ping**, **Rafel**, **Sathiyaraj**, **Smita**, **Sudir**, **Tam**, and **Xiaoya**. I would also like to thank **Hugo**, **Giorgia**, and **Simone**, who endured challenging thesis projects and managed splendidly while having me as an impatient advisor.

My work was not limited to the town of Lund but extended to big cities such as Gothenburg and Stockholm, because of the opportunities to collaborate with wonderful researchers and universities within the SSF-FFI project. The principal investigators, **Björn**, **Carina**, **Göran**, **Inna**, and **Rakel**, and other researchers in the project, thank you for the valuable collaboration which broadened my research area. **Eva**, **Gerard**, **Nikola**, **Timon**, and **Yi**, thanks for helping me understand a bit more about electrochemistry and for the fun times we shared during meetings and courses. There is another SSF project I got involved in and had the chance to work with **Ann**,

Burak, **Matteo**, and other members in the PUSH project. Thank you for exchanging ideas and the collaborative work.

My activities were even extended to outside of Sweden to Denmark. In the NEXTAEC project, I was introduced to the field of water electrolysis where I met other membrane researchers and learned new knowledge. Sincere thanks to **David**, **Mikkel**, **Oluf**, **Sinu**, and many others in the project. Special thanks to **Yifan**, for your help with impedance measurements and set-up.

Luckily, I met friends who made my life outside work colorful and interesting. Heartfelt thanks to **Ping**, **Si**, **Xiaoya**, **Yifan**, **Hailiang**, **Yutang** and **Lu**, **Yuhan** and **Meiyuan**, for spending relaxing time and helping each other in this foreign land. Special thanks to **Chendi** and **Hao**, for lobster fishing, road trip to Norway, hangouts and sleepovers, and authentic food on traditional Chinese holidays. Many thanks to **Niklas** and the **Warlins**, for your great hospitality and warming invitations to julbord every Christmas and adventures at your summer house. Thank you, **Olivier**, for hosting Polymat BBQs, Christmas baking, board games and other fun activities. Thank you, **Huong**, for many hotpots, home-made Vietnamese food and great chats we had.

I want to thank my friends back in China. Among them, **Yiting**, **Xiu**, and **Chenchen**, thank you for the company during many bright and dark times. Thanks go to my schoolteachers, and professors at TGU in Tianjin. Of the many subjects I have studied and liked, it was English and chemistry-related ones that finally brought me here. I would like to express my gratitude to **Prof. Zhou Yang** for supervising me during master's studies and supporting my applications for doctoral positions. Thanks to every doctoral and master's students from the research group in USTB with whom I had the pleasure to share office, corridor, and labs.

My wonderful and worry-free life abroad has been possible because of my supportive and loving parents. They have been taking good care of themselves, and happily living a healthy life so that I can focus on mine. **Changyuan**, my husband, I wouldn't have made this through without you taking in my venting and knowing exactly how to cheer me up. How lucky I am to have met you and to experience a life full of happiness and possibilities! Years ago, I made up my mind to pursue a doctoral degree at a dinner table with my parents-in-law. Their encouragement was one of the most important driving forces. Thanks for the initial nudge and following support. Now I have almost done it.

综上，真诚感谢良师益友和所有家人。

(All in all, sincere thanks to mentors, friends, and my family.)

Finally, this thesis work was funded by Swedish Foundation for Strategic Research (SSF) and Swedish Energy Agency through the FFI program. Financial support from them and Kungliga Fysiografiska Sällskapet i Lund is highly appreciated.

Popular science summary

Polymers belong to a class of large molecules consisting of many repeating units. There are natural polymers including cellulose and silk, as well as synthetic ones, such as polyethylene and polystyrene. Most polymers are good electrical and thermal insulators. Depending on the application, polymers can be made or modified so that they can conduct electrons or ions. Ionomers are ion-conductive polymers which contain positively or negatively charged ionic groups covalently bonded to them. They usually have a powdery or fibrous appearance and have good processability after dispersion or dissolution. From solutions, an ionomer can be fabricated into a flat membrane and used as an ion exchange membrane (IEM). IEMs are soft, transparent materials with a thickness ranging from as thin as plastic wrap to A4 paper. This thesis deals with the design and synthesis of ionomers and the characterization of them as IEMs for energy conversion and storage applications.

The global energy crisis and related environmental issues call for sustainable and green energy solutions to avoid burning fossil fuels. Renewable energy such as solar and wind is abundant but intermittent as they are limited by seasons and regions. To make the best use of such resources, they need to be combined with efficient energy storage technologies. Hydrogen gas (H_2) is a clean and energy-dense fuel. Electricity generated from renewable sources can be used to produce H_2 by water electrolysis, thereby storing the energy as chemical fuel. Water electrolysis is the electrochemical splitting of water molecules into H_2 and oxygen gas (O_2). The reverse reaction consumes H_2 in fuel cells and generates electricity with high efficiency and only water as a by-product. The combination of the two technologies constitutes the key to the H_2 economy, which shows great potential and hope toward global decarbonization.

Fuel cells and water electrolyzer cells are currently under rapid development. Research has shown that alkaline operating conditions have great advantages over acidic ones, including simplicity, low cost, and fast kinetics. The main technical bottleneck of the alkaline devices has been their unsatisfactory performance and lifespan. This is related to the lack of high performing components, such as ionomers and IEMs. The ionomer is used as catalyst binder in the electrodes of the cells, and the IEM separates the electrodes and the reactive gases and, more importantly, conducts ions between electrodes. High conductivity of the ionomer and the IEM is essential for a high performance of the cells, and the durability of these two materials determines the device's lifetime. In an alkaline environment at high hydroxide ion concentrations, especially at high temperatures (60-90 °C), ionomers and IEMs are vulnerable to chemical degradation. Such a degradation is irreversible and detrimental to cell performance, eventually leading to failure of the devices.

Therefore, it is imperative to identify highly conductive and durable ionomers and IEMs to propel the development and commercialization of alkaline fuel cells and water electrolyzer cells. This thesis work exploited a unique polymerization method to prepare ionomers, after which their properties as IEMs were studied. Polymer structures were carefully designed to synthesize materials with enhanced ionic conductivity and chemical stability compared to state-of-the-art. Important structure-property relationships were established, and the overall results provide valuable information for future IEM research and development.

大众科学总结

聚合物材料因其丰富的种类和功能，极大的推动了人类社会的发展。无论是蚕丝，树脂，明胶等天然聚合物还是电木（酚醛树脂），涤纶，人造橡胶等合成聚合物都在人类生产生活中扮演着重要作用。聚合物是由大量重复单元以共价键连接形成的大分子，因此聚合物材料通常是电和热的不良导体并且常被应用于绝缘保护材料。随着社会进步的需求不断提升，可以导通电子的共轭聚合物与对离子具有良好传导能力的离子聚合物材料也应运而生。离子聚合物（离聚物）是含有正或负带电离子基团的聚合物。它们通常具有粉末状或短纤维状外观，并且在分散或溶解后具有良好的可加工性。从溶液中，离子聚合物可以被制作成柔软透明的离子交换膜，厚度从薄如保鲜膜到 A4 纸不等。本论文研究的内容聚焦于离聚物的设计与合成，以及可应用于能量转换和存储装置的离子交换膜的表征。

全球能源危机和环境问题日益严重，人类社会急需可持续的绿色能源解决方案来减少对燃烧化石燃料的依赖。大多可再生能源如太阳能、风能等虽资源丰富，但受季节和地域的限制，其应用具有很强的间歇性。为了充分利用这些资源，它们需要与高效的储能技术相结合。氢气的循环利用是解决这一问题的潜在方法。氢气是一种清洁且高能的燃料。太阳能等可再生能源转化的电力可经由电解水生产氢气而高效地储存为化学能。其中，水电解是水分子电化学分裂成氢气和氧气的过程。其逆反应可应用于燃料电池高效发电，在此过程中氢气被消耗，同时仅生成水作为副产物。由此，上述两种技术的结合构成了氢经济的关键，并可成为实现全球碳中和的巨大推动力量。

目前，燃料电池和水电解槽技术正在快速发展。研究表明，碱性运行条件与酸性相比具有成本低和电极反应更为迅速的优势。碱性设备的主要技术瓶颈是其性能和使用寿命不足，其原因包括缺乏高性能的离聚物和阴离子交换膜。在这些设备中，离聚物可被用作电池电极中的催化剂粘合剂。离子交换膜则可将电极两端和反应气体分开，并在电极之间传导离子。高电导率是上述材料功能的基础，而高性能电池设备对离聚物和离子交换膜的要求除具有高电导率外也包括其长期稳定性。在高氢氧根离子浓度的碱性环境中，尤其是在高温（60-90 °C）下，离聚物和阴离子交换膜容易发生化学降解。这种降解是不可逆的，并且会降低电池性能，最终导致设备失效。因而，这两种材料的耐用性决定了电池的使用寿命。

综上所述，本论文的目的是改进离聚物和阴离子交换膜的电导率和耐用性，以推动阴离子交换膜燃料电池和水电解槽电池的发展和大规模商业化。本论文工作采用独特的聚合方法制备离聚物，并研究了它们作为阴离子交换膜的性能。通过总结当前技术的经验，本论文探讨了其背后的结构-性能关系并提出了改进材料性能的聚合物结构设计策略，据此合成了具有更为优秀的离子电导率和化学稳定性的材料。整体结果为未来的阴离子交换膜研发提供了有价值的信息。

List of appended papers

This thesis is based on the following papers:

I. **Poly(fluorene alkylene) Anion Exchange Membranes with Pendant Spirocyclic and Bis-Spirocyclic Quaternary Ammonium Cations**
Dong Pan, Joel S. Olsson, and Patric Jannasch
ACS Applied Energy Materials **2022**, *5*(1), 981-991

II. **Poly(arylene piperidine) Anion Exchange Membranes with Tunable *N*-Alicyclic Quaternary Ammonium Side Chains**
Dong Pan, Thanh Huong Pham, and Patric Jannasch
ACS Applied Energy Materials **2021**, *4* (10), 11652-11665

III. **Improving Poly(arylene piperidinium) Anion Exchange Membranes by Monomer Design**
Dong Pan, Pegah Mansouri Bakvand, Thanh Huong Pham, and Patric Jannasch
Journal of Materials Chemistry A **2022**, *10*, 16478-16489

IV. **Hydroxide Conducting Membranes with Quaternary Ammonium Cations Tethered to Poly(arylene alkylene)s *via* Flexible Phenylpropyl Spacers**
Si Chen[†], Dong Pan[†], Haiyue Gong, and Patric Jannasch
In manuscript
[†]These authors contributed equally.

V. **Alkali-Stable Anion Exchange Membranes Based on Poly(xanthene)**
Dong Pan, Si Chen, and Patric Jannasch
ACS Macro Letter **2023**, *12* (1), 20-25

My contributions

I. I planned and performed all the experimental work. I wrote the first draft of the paper.

II. I planned and performed most of the experimental work. I wrote the first draft of the paper.

III. I planned and performed half of the experimental work. I prepared the majority of the first draft and revised the manuscript.

IV. I planned and performed some synthesis and characterization work. I took an active part in discussing the results, reviewing, and editing the manuscript.

V. I planned and performed most of the experimental work. I wrote the first draft of the paper.

Publications not included

VI. Asymmetric cycling of vanadium redox flow batteries with a poly(arylene piperidinium)-based anion exchange membrane
Amirreza Khataee, Dong Pan, Joel S. Olsson, Patric Jannasch, and Rakel Wreland Lindström
Journal of Power Sources **2021**, 483, 229202

VII. Electrochemical performance of poly (arylene piperidinium) membranes and ionomers in anion exchange membrane fuel cells
Timon Novalin, Dong Pan, Göran Lindbergh, Carina Lagergren, Patric Jannasch, and Rakel Wreland Lindström
Journal of Power Sources **2021**, 507, 230287

VIII. Ionomer catalyst interaction and effect of solvent ratio on electrochemical oxygen reduction and hydrogen oxidation reaction in alkaline conditions
Roopathy Mohan, Gerard Montserrat Sisó, Dong Pan, Victor Shokhen, Patric Jannasch, and Björn Wickman
In manuscript

IX. Using an ionomer as size regulator in γ-radiation-induced synthesis of Ag nanocatalysts for oxygen reduction in anion exchange membrane fuel cells
Yi Yang, Dong Pan, Junyi Li, Patric Jannasch, Mats Jonsson, and Inna L. Soroka
Submitted to Journal of Colloid and Interface Science (February 2023)

Abbreviations and symbols

Abbreviations

AEM	anion exchange membrane
AEMFC	anion exchange membrane fuel cell
AEMWE	anion exchange membrane water electrolyzer
ASU	6-azonia-spiro[5.5]undecane
AWE	alkaline water electrolyzer
DCM	dichloromethane
DIPEA	*N*,*N*-diisopropylethylamine
DMAc	dimethylacetamide
DMP	*N*,*N*-dimethylpiperidinium
DSC	differential scanning calorimetry
FC	fuel cell
HEM	hydroxide exchange membrane
HEMFC	hydroxide exchange membrane fuel cell
HER	hydrogen evolution reaction
IEM	ion exchange membrane
MEA	membrane electrode assembly
MeI	methyl iodide
mPip	*N*-alkyl-*N*-methylpiperidinium
NMR	nuclear magnetic resonance
NMP	*N*-methyl-2-pyrrolidone
OER	oxygen evolution reaction
PAP	poly(arylene piperidinium)
PEM	proton exchange membrane
PEMFC	proton exchange membrane fuel cell
PEMWE	proton exchange membrane water electrolyzer
PGM	platinum group metal

QA	quaternary ammonium
Qui	quinuclidinium
SEC	size exclusion chromatography
SAXS	small angle X-ray scattering
TFA	trifluoroacetic acid
TFAA	trifluoroacetic anhydride
TFSA	trifluoromethanesulfonic acid
THF	tetrahydrofuran
TGA	thermal gravimetric analysis
TMA	alkyltrimethylammonium

Symbols

$[\eta]$	intrinsic viscosity
σ	ion conductivity
d	characteristic distance
$Đ$	dispersity
q	scattering vector
M_n	number-average molecular weight
T_g	glass transition temperature (by DSC)
$T_{d,\,95}$	the temperature at 5% weight loss (by TGA)

1 Context and scope

Worldwide energy production currently relies on burning fossil fuels which is causing vast greenhouse gas emissions and leads to severe climate impact, including heat waves, extreme weather, rising sea levels, and threatened biodiversity. Since the late 1800s, the world has warmed by 1.1 °C, and the rising temperature needs to be restrained to 1.5 °C for the earth to still be liveable.[1] This requires the emissions to be cut by almost half by 2030, and reach net-zero by 2050. To achieve this, a way to transit from the dependence on fossil fuels to renewable energy sources is in great demand. In fact, renewable energy sources such as solar and wind are highly available and cost-effective all around the globe, yet the use of them is limited because of seasonal and regional factors.[2] Therefore, it is of great interest to efficiently store energy produced from these intermittent resources and distribute it when and to wherever it is needed.[3] Energy storage in the form of chemical fuels offers a high energy density.[4] For example, H_2 has long been identified as a clean energy vector with high energy content, indicating that it could satisfy the large energy demand globally.[5] Meanwhile, it does not require a remake of the whole distribution systems, because the existing grids for gas and oil can be used to distribute the H_2 gas.[4]

To truly contribute to global decarbonization, the production of H_2 needs to be zero-carbon as well. Green H_2 refers to H_2 produced by water electrolysis, where water molecules are split into H_2 and O_2 using electricity with no emissions, i.e., from intermittent renewables (solar and wind).[6, 7] Thus, the energy can be stored in the form of H_2, and can then be used when/wherever it is needed. Another electrochemical device closely related to hydrogen is the fuel cell. It converts the chemical energy of H_2 to electricity with significantly higher efficiency than simple combustion of H_2.[8] Today, fuel cells are widely applied for stationary, portable, and transportation power generation.[9]

Over the years, water electrolysis and fuel cell technologies have achieved great advances and commercially available devices have been introduced for various uses.[10] Scaled-up applications are limited by the high cost of the cell components. Therefore, the current research is steering toward alkaline operation conditions for both devices, because of the fast electrode kinetics and avoidance of expensive raw materials, such as Ir and Pt.[11] The task of adapting all the device components to the high pH environment is demanding and requires efforts from many research fields. One crucial component, the anion exchange membrane (AEM), is presently under extensive research.[12] AEMs are one type of ion exchange membrane (IEM) which are solid polymeric materials separating the electrodes and transporting conductive ions. Their properties largely dictate the efficiency/performance and lifetime of the devices, and are challenged by the high operating pH and temperature of the devices.

The topic of this thesis is the design, preparation, and characterization of AEMs specifically used under alkaline environment, i.e., hydroxide exchange membranes (HEMs). Starting from the molecular design, the work is aimed at developing cationic polymers which are alkali-stable from the molecular viewpoint, and HEMs with complementary properties such as high ionic conductivity and alkaline stability.

2 Introduction

Ion exchange membranes (IEM) are semi-permeable materials which are used as polymer electrolyte membranes in a great variety of electrochemical devices[13], such as water electrolyzers[14], fuel cells[15], and redox flow batteries[16]. They consist of polymers with charged functional groups covalently immobilized. In contact with aqueous solutions, the nature of the functional groups enables selective conduction of ions by dissociation, which divides IEMs into two categories. An IEM with negatively charged groups (anions) conducts cations (mostly protons) and is called a proton exchange membrane (PEM), with the counterpart being an anion exchange membrane (AEM).

In the following sections, low-temperature (< 90 °C) IEM-based electrochemical devices will be briefly described.[17] Such devices typically comprise two electrodes, an IEM acting as a separator and electrolyte sandwiched in-between, as well as an external circuit. The focus is placed on the basic working principles, pros and cons of different types of devices, and more importantly, the requirements of the IEMs. Advances on other components, such as catalyst layers, will not be discussed. Similarly, other devices of the same kind that do not use an IEM as the electrolyte will not be addressed.

An in-depth focus is placed on the AEMs used under alkaline environments, i.e., hydroxide exchange membranes (HEMs), which refers to AEMs where the sole conducting ion is the hydroxide ion. Common polymer and cation structures, transport properties, and especially the challenge of chemical stability of the HEMs will be discussed.

2.1 Electrochemical devices

2.1.1 Water electrolyzers

Water electrolysis is an electrochemical process which consumes electricity to produce H_2 gas by splitting water molecules.[18] It provides a clean solution in response to the energy crisis and fossil fuel depletion. The water electrolyzer comprises an anode, a cathode, and an electrolyte. The selection of electrode materials and electrolyte is wide and depends on the operating conditions of the cell. For example, the alkaline water electrolyzer (AWE) uses concentrated KOH (20-30 wt%) as electrolyte, and is by far the cheapest and most widely applied electrolyzer.[7] The electrodes are typically nickel or cobalt, and in between the electrodes is a porous diaphragm that separates the two reactant gases. The existing distance between the diaphragm and electrodes makes it a gap design.[18] Although the system

is inherently simple, the drawbacks of AWE are a high gas crossover through the porous film, and potential leakage of the caustic KOH electrolyte. More importantly, the gap design leads to high ohmic resistance and limits the maximum current density.[19] To improve the situation, an ion conducting membrane can be employed to replace the non-ionic diaphragm.[20] A PEM based on e.g., perfluorosulfonic acid polymers is sandwiched in-between the two electrodes forming a membrane electrode assembly (MEA), creating a zero-gap design. In this way, the ohmic resistance at the electrode surfaces, as well as the internal resistance of the membrane, can be largely reduced to achieve higher efficiency.[18] However, the highly acidic environment in PEM water electrolyzers (PEMWEs) requires the use of precious platinum-group metals (PGMs), such as Ir and Pt, to catalyze the electrode reactions, which significantly increases the cost. Potentially, this can be circumvented by AEM water electrolyzers (AEMWEs) which operate under alkaline environment in tandem with non-PGM catalysts. Overall, AEMWEs combine the merits of AWE: the faster OER kinetics under alkaline conditions[19] and PEMWE: low surface resistance brought by ion conducting membranes (**Figure 1**).

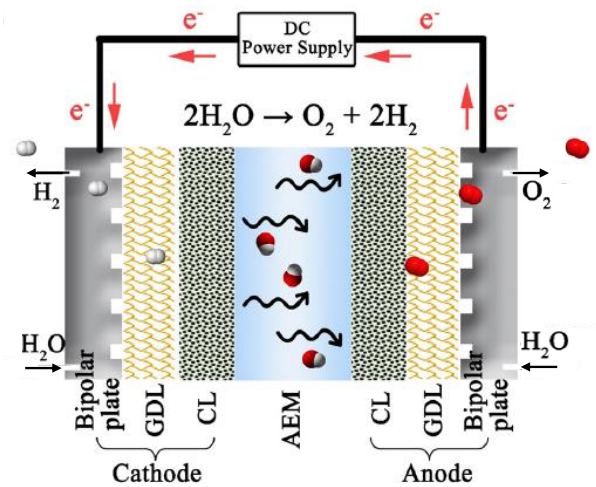

Figure 1. Schematic illustration of an anion exchange membrane water electrolyzer (AEMWE), adapted and modified from Pan et al.[21]

In the process of water electrolysis, the electrode reactions involve the oxygen evolution reaction (OER) at the anode and the hydrogen evolution reaction (HER) at the cathode. Specifically, the reactions under alkaline environment are as follows:

Anode: $4OH^- \rightarrow O_2 + 2H_2O + 4e^-$

Cathode: $4H_2O + 4e^- \rightarrow 2H_2 + 4OH^-$

Net: $2H_2O \rightarrow O_2 + 2H_2$

As can be seen from the electrode reactions, OH^- ions are produced at the cathode and consumed at the anode. The ion transport and water diffusion are facilitated by the HEM and ionomers in the catalyst layer. Therefore, the properties of HEMs play an important role in increasing the performance of AEMWE to become competitive with commercial PEMWEs and AWEs. The HEMs should possess high OH^- conductivity and low gas permeability, as well as efficient water diffusivity. Currently, the HEMs lack a sufficient conductivity, so the circulation of dilute KOH solutions is necessary to supplement OH^- ions at the anode and reach high performance by decreasing electrode and cell resistance.[21, 22] However, this adds potential complications and cost to the system, and more importantly, it challenges the chemical integrity of the HEMs.[7] Ultimately, the availability and low cost of deionized water makes the water-fed systems the overall best choice, which means that extensive research on different cell components is needed, especially on the HEMs.

2.1.2 Fuel cells

Fuel cells (FCs) convert chemical energy stored in a fuel (e.g., H_2 gas) to electrical electricity *via* electrochemical reactions. It is a promising technology to aid in the shifting from a fossil-based economy to a H_2 economy, thus contributing to global decarbonization.[23] First demonstrated in the 18th century, FCs have advanced significantly and are nowadays seen in portable, transportation and stationary applications.[9] FC-powered vehicles using H_2 as a fuel emit much less (almost zero) CO_2 gas in comparison with conventional combustion engines run on fossil fuels. The high energy density of H_2 offers increased efficiency at potentially lower cost, especially for long-distance transportation.[24] Moreover, compared to the relatively time-consuming charging of electric vehicles, fuel cell vehicles take much shorter time to refuel.[24] In stationary applications, FCs enable a long-term power supply as long as the fuels are continuously fed.

FCs can operate at various temperatures ranging from 60 to 1000 °C and are generally characterized by the type of electrolyte and fuel. There are phosphoric acid fuel cells, alkaline fuel cells,[25] molten carbonate fuel cells,[26] solid oxide fuel cells,[27] and polymer electrolyte membrane fuel cells,[15] which is the most relevant type of FC for this thesis work. The polymer electrolyte is typically a solid IEM. Due to the compact configuration, low temperature, and avoidance of liquid electrolytes, this technology is especially attractive for transportation applications. Depending on the operation environments and the nature of the corresponding IEM, polymer electrolyte membrane fuel cells can be classified into two main categories: proton exchange membrane fuel cells (PEMFCs) and anion exchange membrane fuel cells (AEMFCs). Specifically, AEMFCs in which CO_2 is excluded and OH^- ions act as the only conducting species are referred to as hydroxide exchange membrane fuel cells (HEMFCs) throughout this thesis work.

Proton exchange membrane fuel cells

PEMFCs are the most mature FC technology, and commercial products are widely applied. Especially, PEMFCs show formidable potential as a replacement for internal combustion engines, because of the high efficiency, high power density and rapid start-up. For instance, PEMFC-powered trucks are more cost-effective than electric trucks for transportations at long ranges (> 483 km).[24] The electrode reactions of a PEMFC are as follows.

Anode: $2H_2 \rightarrow 4H^+ + 4e^-$

Cathode: $O_2 + 4H^+ + 4e^- \rightarrow 2H_2O$

Net: $2H_2 + O_2 \rightarrow 2H_2O$

One important factor for the success of PEMFCs is the well-developed PEMs, which are a class of perfluorinated sulfonic acid (PFSA) membranes with a representative polymer structure shown in **Figure 2**. Such membranes were first invented by DuPont and are known by the trademark Nafion.[28] Nafion polymers consist of a hydrophobic fluorinated backbone and super-acidic PFSA groups. This combination promotes phase separation and gives Nafion high proton conductivities, up to 90 mS cm^{-1} at 20 °C (fully hydrated).[29] The proton conductivity is also superior at low relative humidity, which is challenging for other types of PEMs reported in the literature. However, Nafion suffers from poor mechanical stability due to its low glass transition temperature (T_g),[30] and easy dehydration at high temperature. Moreover, it is a quite expensive material to produce and the recycling is difficult.[31] This, together with the essential platinum-based catalysts for PEMFCs, significantly increases the cost of the device and limits the large-scale commercialization of fuel cell vehicles.[32]

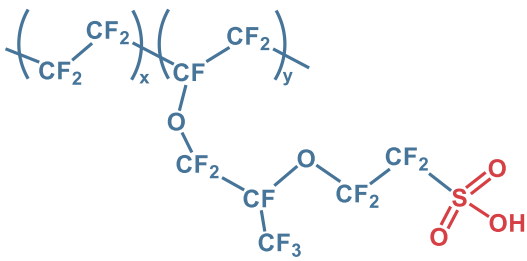

Figure 2. The chemical structure of Nafion.

Hydroxide exchange membrane fuel cells

To find a cost-effective alternative to PEMFCs, recent years have witnessed extensive research efforts invested in the new and promising area of HEMFCs.[33] **Figure 3** illustrates essential components of an HEMFC. Similar to AEMWEs, the high pH operating media of the cell provides faster kinetics of the electrode

reactions, which potentially gives the option to use non-platinum-group catalysts such as nickel or silver.[34] The electrode reactions of an HEMFC are described as following:

Anode: $2H_2 + 2OH^- \rightarrow 4H_2O + 4e^-$

Cathode: $O_2 + 2H_2O + 4e^- \rightarrow 4OH^-$

Net: $O_2 + 2H_2 \rightarrow 2H_2O$

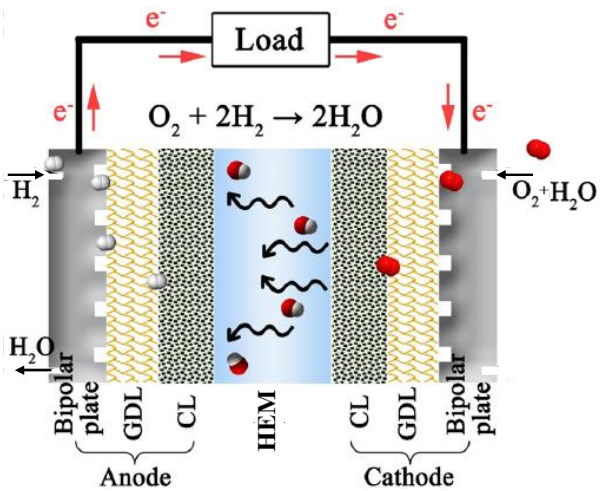

Figure 3. Schematic illustration of an hydroxide exchange membrane fuel cell (HEMFC), adapted and modified from Pan et al.[21]

Over the past two decades, the development of HEMFCs has made substantial progress. High performances with peak power densities between 1.5-3.4 W cm^{-2} (operated under H_2/O_2 at 80-95 °C)[35-40] have been reached. These values approach that of the advanced PEMFCs. Still, the long-term durability of HEMFCs is inferior and remains a challenge, which is closely related to the stability of the cell components, including the electrodes and the HEM in the MEA. For example, in a high pH environment, the HEM contains strongly basic and nucleophilic OH^- ions. The highly chemically aggressive OH^- ions tend to attack the HEM and cause structural degradation of the HEM polymer. The degradation is often a loss of cations, which results in loss of ion conductivity and cell performance. It may also be scission of the polymer backbone, leading to loss of mechanical strength of the HEM and failure of the cell.[34] Overall, achieving a high durability of the HEM is a great challenge in the development of HEMFCs. Even so, it has been seen that other components in the cell may degrade degradations in the cell much faster than the HEM.[41] Studies have shown performance decay of the cells after short-time operation (< 200 h), [12, 42] while post-mortem analysis suggested an intact chemical

structure of the HEM. Even though, the development of alkali-stable HEMs is still necessary to ensure long-time operation (> 2000 h) of the HEMFCs. The durability of the HEMs is discussed more in detail in Section 2.2.4.

The water management of an HEMFC is more complicated compared with PEMFCs.[43] It arises from the larger imbalance of the water content between the electrodes, caused by the difference in consumption/generation of water molecules in the electrode reactions. Not only is water generated at the anode, the OH^- ions also carry water molecules with them as they are transported to the anode, creating a tendency for anode flooding. In the meantime, water is consumed at the cathode. If water is not sufficiently supplied by diffusion through the HEM, from e.g., the anode, cathode dry-out poses a great risk for the chemical stability of the HEM. Several strategies have been shown effective in improving water management by employing a relatively hydrophobic anode and hydrophilic cathode by adjusting the properties of the ionomers,[40] or decreasing the HEM thickness to even merely 5 μm.[35, 41] This again requires a sufficient mechanical strength of the membrane to guarantee stable cell operation.

2.2 Hydroxide exchange membranes

In HEMFCs and AEMWEs, HEMs play a vital role in separating the electrodes, conducting ions, and forcing the electrons to go through the external circuit. It should have a high conductivity to ensure a high power density of the devices, as well as low gas permeability to prevent reactant gas crossover. The conductivity is related to the ion exchange capacity (IEC) of the HEM, which is defined as the mol of cationic groups per gram of dry membrane. In principle, the higher the IEC, the more charge carriers are available to conduct ions and reach high conductivity. HEMs conduct OH^- ions by ion dissociation and solvation, making the water content of the HEM another important factor to consider. A sufficient water uptake is essential for efficient ion transport. However, an excessive water content (e.g., > 100%) causes dimensional swelling of the membrane, which potentially impairs the mechanical strength and results in membrane disintegration and device failure. Also, above a certain concentration, the high water uptake dilutes the charge carrier (OH^-) and decreases the conductivity. Therefore, a high conductivity at low hydration levels is highly desired for the HEM.

2.2.1 Ion transport and morphology

Hydrated protons in aqueous systems are transported *via* structural diffusion (Grotthuss mechanism) and vehicular diffusion.[44] Structural diffusion involves a continuous interconversion of solvated hydronium (H_3O^+) complexes: $H_9O_4^+$ and

$H_5O_2^+$, driven by fluctuations of the hydrogen bond network in the solvation shells.[45] A hydrated OH^- had been regarded as a H_2O molecule missing a proton, and this 'proton-hole' concept was long applied to explain OH^- transport mechanism.[46] Using simulation methods, Tuckerman et al. identified OH^- hydration complexes which have little structural similarity to H_3O^+ complexes, and proposed an alternative mechanism to that of the 'proton-hole' picture for the OH^- ion transport.[45] The difference in solvation structures is an explanation for the lower mobility of the OH^- ion compared to the proton in aqueous solutions, which is of particular relevance in the development of HEMs. The relatively lower OH^- ion mobility makes it inherently challenging for HEMs to reach as high ion conductivity as PEMs at an equal IEC. In addition, the typical cationic groups in HEMs, e.g., quaternary ammoniums (QAs), are weak bases ($pK_b \sim 4$) in comparison with the sulfonic acid groups ($pK_a \sim -1$) in PEMs which are strongly acidic.[47, 48] This presents a considerable barrier for efficient ion dissociation and conduction in the alkaline system.[47] Especially, the degree of dissociation declines at lower hydration level. Lastly, the potential CO_2 contamination from air results in formation of carbonate and bicarbonate ions with even lower mobility which further restricts the ion conductivity.[34, 49, 50]

As mentioned above, increasing the ionic content (IEC) of an HEM essentially promotes ion conductivity, but this may come at the expense of mechanical integrity. Another factor that influences the conductivity is membrane morphology. On the nanoscale, the hydrophobic polymer backbone and the hydrophilic cations typically separate into two domains. Upon hydration, the hydrophilic domains formed by the aggregated cations overlap and create interconnected conducting channels filled with water to facilitate efficient ion transport.[34] This type of efficient phase separation morphology is believed to be the reason for the high ion conductivity of Nafion.[28] Similarly, this positive effect can be expected for HEMs if a distinctly phase-separated structure is formed. Unlike the highly fluorinated backbone of Nafion, HEMs are commonly based on hydrocarbons which are far less hydrophobic, making it more difficult for HEMs to phase separate. To improve the situation, strategies such as developing block copolymers,[42, 51] 'comb-shaped' polymers,[52-54] and employing multiple cations[55-58] have been utilized and shown successful results. HEMs with a distinct phase separation have been able to achieve high OH^- conductivity at a relatively low IEC and water uptake, compared to HEMs without such a feature.[59] To date, several HEMs with a high OH^- conductivity above 200 mS cm^{-1} at 80 °C under 100 RH% or immersed state have been reported.[57, 60]

2.2.2 Polymer backbone

The polymer backbone constitutes the molecular structure of an IEM. It strongly influences IEM properties such as solubility, morphology, mechanical flexibility

and strength. Taking the aforementioned Nafion as an example, the superior conductivity of this membrane is attributed to the distinct micro-phase morphology induced by the high hydrophobicity of the backbone in contrast to the hydrophilic superacidic sulfonate groups, while the often inadequate mechanical strength and low T_g is caused by the high flexibility of the backbone. Switching to alkaline media from acidic brings new challenges for the polymer backbones in terms of chemical stability. Poly(aryl ether sulfone)s are widely used as PEMs, and show excellent alkaline stability when non-ionic.[61] However, once electron-withdrawing cations are introduced, the polymer tends to undergo backbone cleavage by hydrolysis of the ether bond, and the reaction is accelerated by additional electron-withdrawing substituents in the vicinity.[61, 62] Therefore, despite the good solubility brought by the flexible C-O bond, research has steered toward preparing HEMs based on ether-free polymer backbones, such as poly(olefin)s,[35, 63-65] poly(phenylene)s[66, 67] and poly(imidazole)s.[68-70]

Ether-free polymers for HEM applications can be synthesized by various synthetic methods including Diels-Alder polymerizations,[71] metal-catalyzed coupling reactions,[72] cyclo-polycondensations,[73] ring-opening metathesis polymerizations[74] and superacid-mediated polyhydroxyalkylations.[75-78] Some representative polymer structures are shown in **Figure 4**.

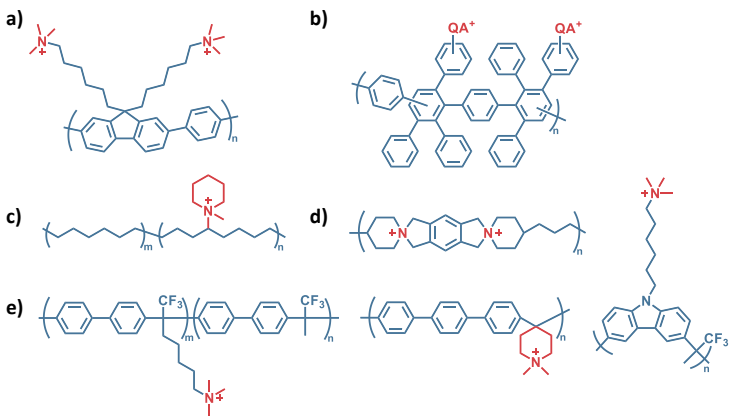

Figure 4. Examples of molecular structures of HEMs based on ether-free cationic polymers.

2.2.3 Cations

The cations are of great importance as the functional ion-exchange groups of an HEM. Their chemical structures largely influence properties such as water uptake, conductivity, and stability. Cations with a wide variety of structures have been investigated for HEMs, including imidazolium,[79, 80] guanidinium,[81, 82] phosphonium,[83] QAs,[84-86] and organometallic species.[87-89] Examples of cationic

groups are illustrated in **Figure 5**. Among them, QAs are the most applied ones owing to their low cost and ease of synthesis.[90, 91]

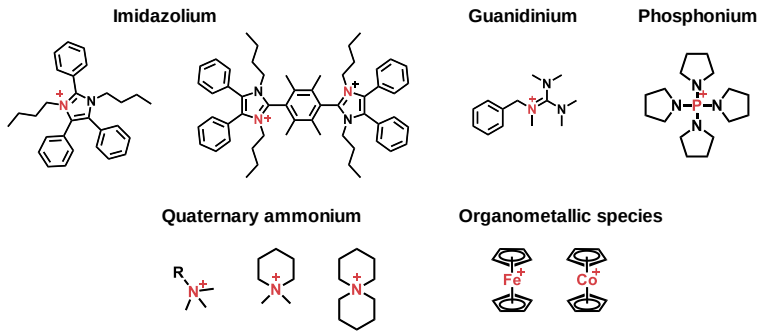

Figure 5. Representative molecular structure of anion-exchanging cationic groups.

Under high pH environment at elevated temperatures, QA cations are prone to degrade, triggered by the highly nucleophilic and basic OH^- ions. Several proposed degradation mechanisms of a QA cation are illustrated in **Figure 6**. The degradation pathways include, but are not limited to, nucleophilic substitution and Hofmann β-elimination.[33] Other mechanisms are known depending on the chemical structure of the cation. In addition, the chemical environment of the QA cations plays an important role in its stability,[33, 84] e.g., the hydration number,[92] the OH^- concentration and temperature. For instance, it has been shown that benzyltrimethylammonium (BTMA) cations are prone to degradation *via* nucleophilic substitution at the benzylic position in alkaline environment, making the cation appeared to be an unsuitable functional group for HEMs.[86] However, recent studies showed that the alkaline stability of the cation is significantly affected by the hydration level of the cation and the OH^- ions. This was explained by the fact that the nucleophilicity and basicity of the OH^- ions are influenced by its degree of solvation.[93, 94]

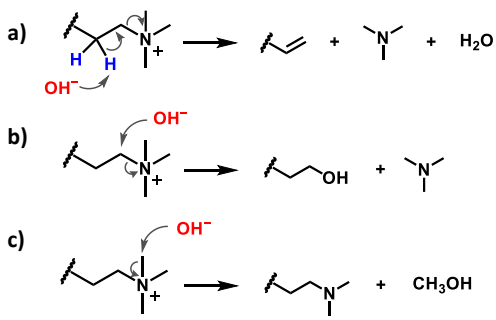

Figure 6. Degradation mechanisms of a QA cation by (a) Hofmann elimination (E_2) at β-proton and (b-c) nucleophilic substitutions (S_N2) at α-carbons.

QA cations with *N*-alicyclic structures have recently emerged and received increasing attention.[86, 95] In a pioneering study, Marino and Kreuer investigated the lifetime of various cationic model compounds and discovered the excellent alkaline resistance of *N*,*N*-dimethylpiperidinium (DMP) and 6-azonia-spiro[5.5]undecane (ASU).[86] This was explained by the low ring strain of the six-membered ring and the high activation energy required for the transition state during Hofmann elimination. Instead, nucleophilic substitution at the methyl group was the primary degradation pathway for the DMP cation. Due to the absence of such methyl groups, the ASU cation showed a longer half-life under the investigated condition.[86] This has encouraged research groups to explore ways to utilize these cations, and promising results have been reported.[73, 96-98] Therefore, DMP and ASU cations were selected as the cation of choice in this thesis work. The possible degradation pathways and degradation products of the two cations are illustrated in **Figure 7**.

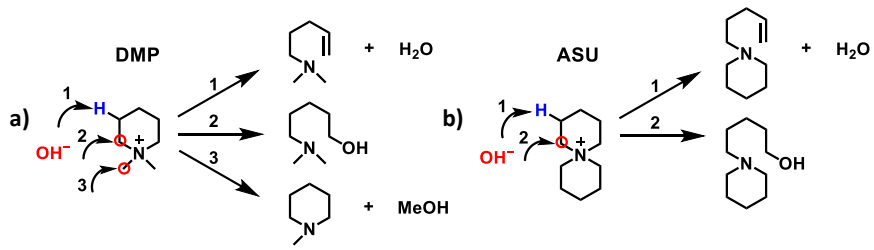

Figure 7. Possible degradation reactions of the (a) DMP and (b) ASU cation by OH^- ions. Reaction 1: Hofmann elimination. Reaction 2 and 3: nucleophilic substitutions. In the study of Marino et al.,[86] reaction 3 and 2 were found to be the main degradation pathway of the DMP and ASU cations, respectively.

2.2.4 Durability of the HEMs

The chemical durability of an HEM is an important topic in the research field.[99-101]As discussed above, both the cation and the polymer backbone of an HEM are susceptible to chemical degradation by the OH^- ions. Moreover, research has shown that precisely how the cations are connected to the polymer has a great impact on the stability of the cation and the HEM. For instance, the aforementioned DMP and ASU cations show excellent chemical resistance when studied as small molecule model cations.[86] However, when they are incorporated into a polymer, the rigidity of the *p*-terphenylene backbone imposes distortions of the cation ring conformation.[76] This lowers the activation energy of the transition state of the degradation reaction, resulting in a reduced alkaline stability.[76] For example, after immersion in 2 M aq. NaOH at 90 °C for 15 days, structural changes of a DMP-functionalized HEM (only the cations) were detected by ^{1}H NMR spectroscopy. In this case, the DMP cation was found to have degraded mainly *via* Hofmann elimination reactions,[76] which is in contrast to the observation of the small molecule model cation, where methyl substitution was the dominating degradation pathway.[86]

In another study, an HEM carrying the ASU cation was found to be even less stable than the DMP counterpart,[96] despite the superior stability of the former cation in the model compound study.[86] These findings demonstrate the importance of studying the cation/polymer arrangement in order to find alkali-stable HEMs.

The durability of HEMs is commonly studied *ex-situ* by immersing samples in alkaline solutions at various molarity and temperature. After the treatments, the remaining IEC, ion conductivity, and mechanical properties of the HEMs are evaluated to assess their chemical stability. In addition, structural analysis of the degraded samples helps to establish the active degradation mechanisms, gaining insight about pathways toward rational molecular designs for alkali-stable structures. On the other hand, *in-situ* durability evaluations are more complicated due to the complex operating environment involving, e.g., variation in hydration levels[92, 102] and pressure, as well as the possible presence of reactive oxygen species.[103-105] For example, the resistance of HEMs toward oxidative degradation has been studied less extensively and needs more attention.[41]

Strategies to improve the chemical stability of the HEMs involve introducing flexible spacers,[55, 106] moieties with multiple cations,[107] and crosslinking.[108, 109] In addition, mechanical properties of the HEMs can be enhanced by reinforcement[110, 111] and blending.[112] Overall, the durability of HEMs, including the cations and the polymer backbone, is of paramount importance when designing HEMs.

2.3 Approach and aim

With alkali-stable polymer backbones and cations identified from literature as a starting point, this thesis work focused on finding an ideal polymer/cation arrangement with the goal to prepare HEMs with high chemical resistance. All the polymers were designed and synthesized by using superacid-mediated polyhydroxyalkylations and post functionalizations. The synthesis steps were kept uncomplicated, although in some cases it was necessary to synthesize new monomers in order to realize the desired polymer structure. The successfully prepared polymers were fabricated into HEMs, which were characterized in terms of water uptake, ionic conductivity, thermal stability, and chemical resistance. HEMs with desirable properties were selected for *in-situ* applications in fuel cells and water electrolyzers, although included as part of this work. **Figure 8** shows representative polymer structures of the HEMs presented in the appended papers.

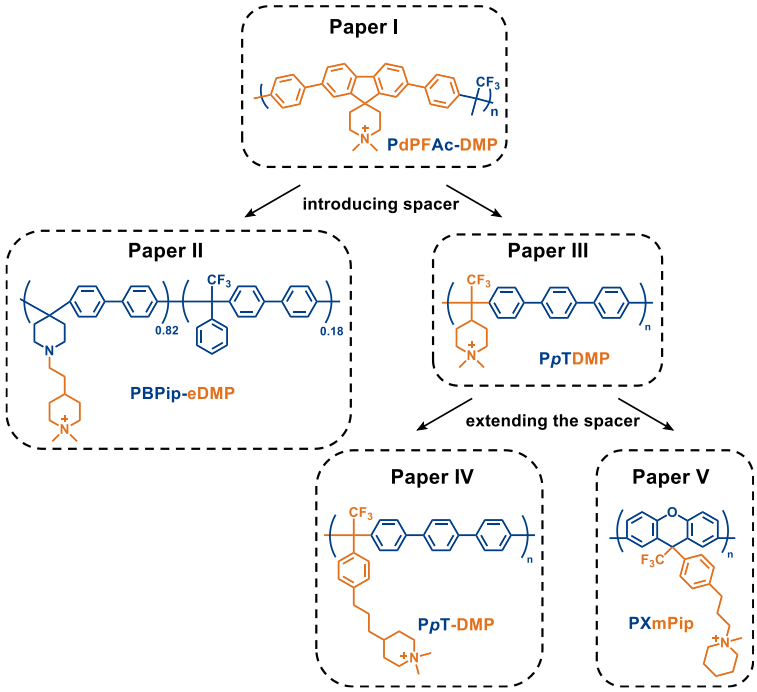

Figure 8. Summary of the thesis work in the form of polymer structures in the discussed appended papers.

3 Experimental methods

This chapter presents the experimental methods used in this thesis work, including the synthesis and characterization methods.

3.1 Synthesis

3.1.1 Polymer synthesis

In this thesis work, the polymerization methods used were based on superacid-mediated polyhydroxyalkylation reactions. The term is derived from hydroxyalkylation reactions, which generally refer to Friedel-Crafts type condensations of aldehydes and ketones with electron-rich arenes in acidic media. The reaction involves the formation of intermediate carboxonium ions. In some cases, such ions can further interact with strong Brønsted or Lewis acids, generating dications known as superelectrophiles with substantially enhanced reactivity.[113] This is called superelectrophile activation and was proposed by Nobel Laureate Olah and co-workers. Ever since, the utilization of superelectrophiles have shown great success in preparation of condensation monomers as well as polymers.[114-117] The mechanism of a typical hydroxyalkylation reaction is depicted in **Scheme 1**.

Scheme 1. Mechanism of the hydroxyalkylation reaction between a ketone and an arene in acid media. k_1 and k_2 are reaction constants.

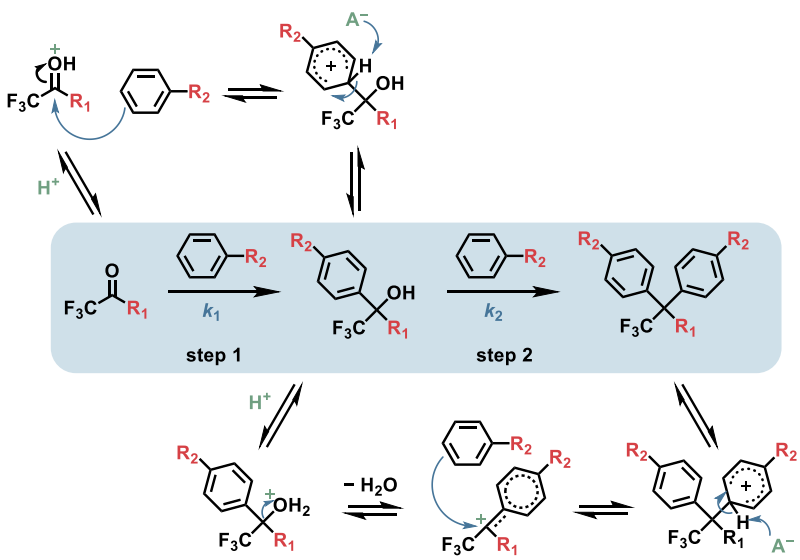

In superacidic media, e.g., trifluoromethanesulfonic acid (TFSA), the reaction proceeds in two consecutive steps. First, the superacid protonates the carbonyl group of the ketone or aldehyde, forming a carboxonium ion. The ion then condenses with an arene compound, producing an intermediate carbinol of which the C-O bond breaks in the next step, generating a carbocation which reacts with a second arene. The rate constants (k_1 and k_2) of the two steps are affected by the structure of the reactive compounds and the reaction conditions. For example, k_1 is related to the basicity and electrophilicity of the carbonyl group, as well as the acid strengths. In addition, an increase in nucleophilicity of the aromatic compound increases k_1. It also increases k_2 due to stabilization of the carbocation in the second step. k_1 and k_2 are also related to the acidity of the reaction media which may even selectively result in either mono- or diaryl product.[118] For example, Ueda et al. demonstrated in several model reactions that when applying an equimolar ratio of the ketone, arene and TFSA, only the diaryl product was found. As the ketone/TFSA ratio increased, monoaryl carbinol started to appear in a quantitative yield when the ratio was above 7.[119]

The synthesis of polymers using the hydroxyalkylation mechanism and superelectrophilic activation was first reported by Zolotukhin et al. They identified that isatin can be doubly protonated by TFSA, and that the resulting superelectrophile readily condenses with aromatic compounds affording poly(arylene oxindole)s with high molecular weight.[116] Since then, the family of polymers prepared using this polymerization method has significantly expanded involving a wide range of carbonyl and aromatic compounds.[120-125] The polymerization is efficient and can lead to high molecular weight product using stoichiometric monomer feed ratio. It was found that the rate of polymerization can be dramatically increased by an imbalanced stoichiometric feed ratio with an excess of the ketone monomer in the cases where $k_1 < k_2$.[118, 126] The reason lies in the higher reactivity of the carbinol intermediate than the carbonyl monomer. The stoichiometric imbalance also results in polymer products with higher molecular weights, which is particularly beneficial when used as HEM precursor polymers. It is however worth to note that a too large excess of the carbonyl monomer may lead to cross-linked, insoluble polymers through side reactions.[118]

Ketone monomers bearing electron-withdrawing groups such as trifluoromethyl groups (-CF_3) are especially interesting to employ in polyhydroxyalkylations.[127, 128] The inductive effect of -CF_3 groups enhances the electrophilicity of the carbonyl group, lowers the activation energy to form the carboxonium ion. This not only facilitates reactions which otherwise might not happen, but also increases the overall polymerization rate and possibly also the molecular weight. Moreover, the presence of -CF_3 groups enhances the thermal stability and glass transition temperature (T_g) of the product polymer. Therefore, when it comes to the monomer synthesis in this thesis work, the -CF_3 group is an essential part of the molecular design, which will be presented in detail in the following section.

3.1.2 Monomer and side group synthesis

Arene monomer

In paper I, a fluorene-based compound carrying a secondary piperidine (dPFPip) was designed (**Scheme 2).** The synthesis was carried out starting with a Suzuki coupling to prepare diphenyl-9,9-*H*,*H*-fluorene (dPHF) according to a previous report.[129] Next, dPHF was reacted with *N*-boc-*N*,*N*-bis(2-chloroethyl)amine using a lithium bis(trimethylsilyl)amide solution as base, constructing a spirocyclic compound including the central fluorene ring and *N*-protected piperidine ring. The reaction was performed first at 0 °C using an ice bath then allowed to proceed at room temperature, during which N_2 protection was applied. To ensure complete conversion, the reaction was monitored by ^{1}H NMR spectroscopy. When the C-9 protons (at δ = 4.06 ppm in $CDCl_3$) were fully substituted, the reaction was stopped by evaporation of solvents. The acquired intermediate compound dPFPip-Boc was purified by stirring the orange-colored solid in water at 50 °C. To remove the Pd catalyst residue from the Suzuki coupling reaction, dPFPip-Boc was first dissolved in dichloromethane (DCM) and mixed with Celite. Then the mixture was quickly washed through a silica gel column using DCM. After an effective deprotection reaction in trifluoroacetic acid (TFA) and DCM, dPFPip was obtained as a pinkish powder with a high yield (81%).

Scheme 2. Synthetic route toward (a) dPFPip (Paper I) and (b) the non-phenylated derivative FPip.

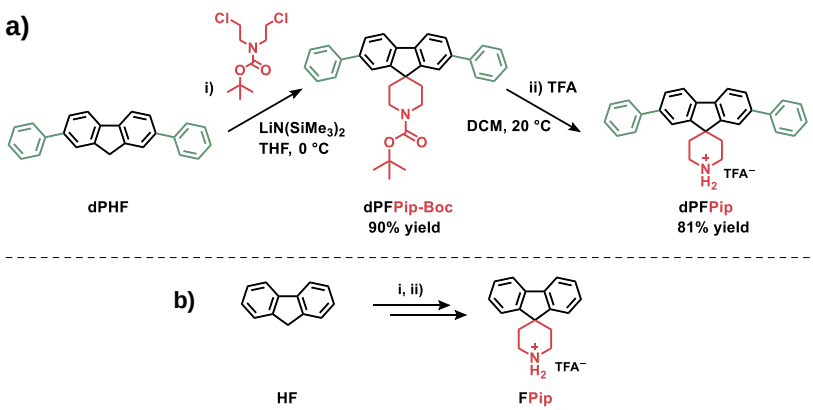

Similar reactions were conducted on 9,9-*H*,*H*-fluorene (HF). The corresponding product FPip was prepared without any issues and its molecular structure was confirmed with ^{1}H NMR spectroscopy. However, polyhydroxyalkylations using FPip and 2,2,2-trifluoroacetophenone failed to form polymers with sufficient molecular weight and good film-forming properties, even after many attempts and optimizations. Therefore, only polymers based on dPFPip were prepared and studied further.

Cationic side groups

In paper II, three cationic compounds were synthesized as grafting agents (**Scheme 3**). The compounds are bromoalkylated cations with an interstitial alkylene spacer of either 1 or 2 carbon atoms. Piperidine-containing alcohols were used as starting materials and the synthesis comprised of i or i') conversion of the piperidine units to DMP or ASU cations, *via* quaternization or cycloquaternization reactions using methyl iodide (MeI) or 1,5-dibromopentane, respectively, and ii) replacement of the hydroxyl groups by bromines by stirring the intermediate product in aq. HBr. The second reaction was kept for 3 days to achieve complete conversion of the alcohols. Despite the long reaction time and large excess of Br^- in the reaction system, a mixture of Br-eDMP and I-eDMP (denoted as X-eDMP in **Scheme 3**) was obtained, as shown by ^1H NMR spectroscopy. This was perhaps caused by the possible residues of NaI salt in the reaction solution. Nevertheless, this did not affect the subsequent functionalizations of the polymers, since the grafting compounds were fed in a large excess up to 5 equiv.

Scheme 3. Synthetic route toward DMP- and ASU-functionalized side groups in Paper II.

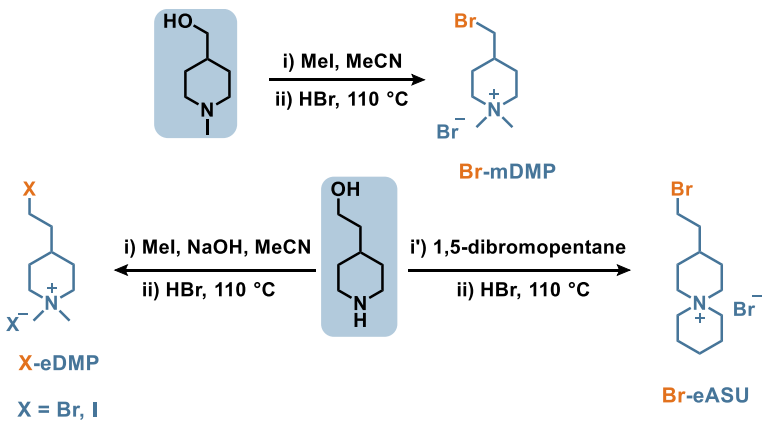

Ketone monomers

Trifluoromethylketones are reactive monomers used in polyhydroxyalkylations. A rational design of a ketone monomer enables successful preparations of polymers with desired molecular structure and cationic arrangement. In this thesis work, three ketones were synthesized using two different pathways (**Scheme 4**). 2,2,2-Trifluoro-1-(4-piperidine)ethanone (TFPip) in Paper III was prepared by direct conversion of a carboxylic acid substrate. 1-(4-Piperidyl)-3-(trifluoroacetylphenyl)-propane (TFAp-Pip) and 1-bromo-3-(trifluoroacetylphenyl)-propane (TFAp-Br) were synthesized *via* Friedel-Crafts acylations in Paper IV and V.

TFPip was synthesized in two steps starting from 4-piperidinecarboxylic acid. First, the carboxylic acid group was reacted with trifluoacetic anhydride (TFAA) in the presence of pyridine, and then went through hydrolysis/decarboxylation in water. In the meantime, the piperidine group first underwent *N*-trifluoroacetylation and then cleavage during the hydrolysis. ^{1}H NMR spectroscopy of the intermediate product revealed that the cleavage was only partial, so the additional hydrolysis in aq. HCl was necessary to finally obtain TFPip as a hydrochloride salt. Pure TFPip was collected after recrystallization in acetonitrile.

Scheme 4. Synthetic route toward ketone monomer (a) TFPip (Paper III), (b) TFAp-Pip (Paper IV) and (c) TFAp-Br (Paper IV and V).

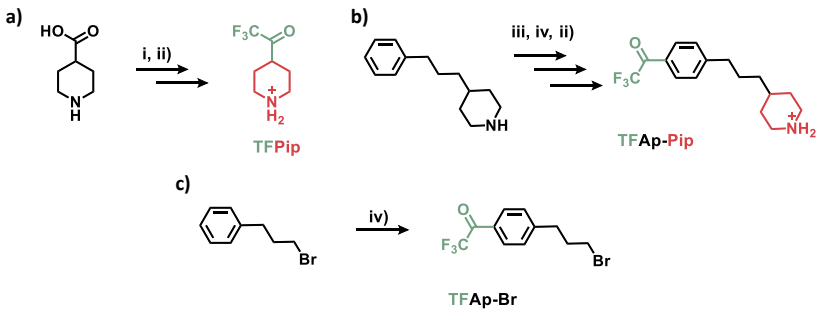

Key: (i) TFAA/pyridine, toluene, 0-50 °C; then H_2O, 0-45 °C; (ii) aq. HCl, 100 °C; (iii) TFAA, DCM, 25 °C; (iv) anhydrous $AlCl_3$, TFAA, DCM, 0-25 °C.

The synthesis of TFAp-Pip started with *N*-trifluoroacetylation of 4-(3-phenylpropyl)piperidine in TFAA and DCM. This was done to deactivate the piperidine group, which was otherwise found to strongly interact with TFAA in the subsequent Friedel-Crafts acylation and decrease the reaction yield. With the pre-treatment, the yield of the later acylation was raised from less than 50% to over 80%. After purification by solvent extraction and silica column chromatography, the intermediate compound was hydrolyzed in aq. HCl. The complete hydrolysis was achieved by repeatedly treating the compound with acetonitrile and aq. HCl, respectively, and TFAp-Pip was acquired in the hydrochloride salt form after recrystallization in acetonitrile. Notably, NMR analysis revealed a majority of TFAp-Pip in the geminal diol form.

TFAp-Br was prepared in one-step followed by a simple workup using a modified procedure from a recent publication.[130] The acylation reaction on 1-bromo-3-phenylpropane was performed in a highly diluted system, in order to prevent potential displacement of the bromine atom. During the reaction, the color of the solution turned from yellow to purple. After 2 h, extraction using water and ethyl acetate, followed by distillation at 160 °C under vacuum gave TFAp-Br as a colorless liquid in a yield over 92%.

3.1.3 Polymer functionalization and quaternization

One important characteristic of the cationic polymers in this thesis is that they are functionalized with QA cations. Due to the formation of a QA cation, the functionalization reaction is often referred to as quaternization reactions throughout this work. In general, it is an S_N2 reaction between an amine and an alkyl halide. Depending on the specific polymer structure, the reaction takes place either on secondary piperidines (**Scheme 5a**), *N*-methyl piperidines (**Scheme 5b**) or bromine atoms of a polymer (**Scheme 5c**). Specifically, the use of a base is necessary to facilitate quaternizations of a secondary piperidine. For example, *N*,*N*-diisopropylethylamine (DIPEA) was employed together with 1,5-dibromopentane to form the ASU cation by cycloquaternization. In all other cases necessary, K_2CO_3 was used. The reaction conditions were adjusted according to the specific reactants. For example, quaternizations involving MeI were performed at room temperature and the reaction vessel was covered with aluminum foil to avoid light-induced degradation of MeI. Cycloquaternization of a secondary piperidine ring was facilitated by heating to 80 °C, and the reaction was kept at low polymer concentration (around 2.5 wt%) to suppress intermolecular crosslinking and promote intramolecular ring closure. In the case of substituting a bromine with a QA, the reaction was either conducted at 40 °C with trimethylamine/water solution, or with *N*-methylpiperidine and quinuclidine at 85 °C. Solvents were chosen according to the solubility of the precursor polymers and the product. Typically, dimethylacetamide (DMAc), dimethyl sulfoxide (DMSO), *N*-methyl-2-pyrrolidone (NMP) or mixtures of the latter two were used.

Scheme 5. Quaternization of piperidine with alkyl halides (a and b), and alkylated bromide with amines (c) to form QA cations.

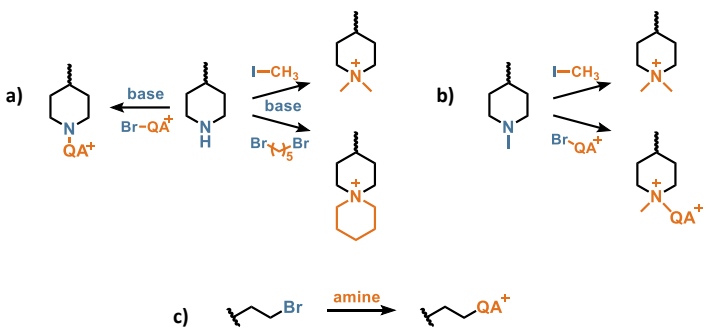

3.1.4 Membrane preparation

HEMs were prepared by solution casting in a ventilated oven at 80 °C. Cationic polymers in the Br^- or I^- form were dissolved into DMSO or NMP to prepare a 5

wt% solution. The solutions were passed through a syringe-driven Teflon filter (Millex LS, 5 μm) onto glass petri dishes (Ø = 5 cm). The dishes were placed in the oven for 48 h until no solvent was left. DI water was added to the dishes to hydrate the membrane for ease of detachment, and then the membranes were gently peeled off, ion-exchanged to the Br^- form in aq. NaBr solutions if they were in the I^- form after functionalization. Then the membranes were stored in DI water prior to analysis and characterizations. Ion-exchange to the OH^- form was done by immersing membrane samples in 1 M aq. NaOH for at least 48 h, during which the alkaline solution was refreshed three times. After ion-exchange, the samples were rinsed with degassed DI water quickly and repeatedly until the water reached neutral pH. The vessels with OH^--containing membranes were always placed in a desiccator under N_2 protection, to avoid CO_2 contamination.

3.2 Characterization methods

3.2.1 Polymer characterizations

Nuclear magnetic resonance (NMR) spectroscopy

The chemical structure of the synthesized compounds was confirmed using NMR spectroscopy on a Bruker DRX400 spectrometer. ^1H, ^{13}C and ^{19}F NMR spectra were recorded at 400, 101 and 376 MHz, respectively. $CDCl_3$ (δ = 7.26 ppm) or DMSO-d_6 (δ = 2.50 ppm) was used as solvents. In the latter case, the spectra were also recorded with addition of 5-10 vol% TFA. TFA protonates the residual water in the NMR sample and reveals proton signals of the polymers otherwise hidden behind the broad water signal at δ = 3.30 ppm. Moreover, it protonates any secondary or tertiary amines present in the sample. These amines either stem from incomplete quaternization reactions, or from degradation reactions after alkaline treatment of the HEM samples, all giving rise to signals above 9 ppm. The absence of the former amines helps to assure the completion of the quaternization reactions, and the revealed amine signals from the degradation products can be used to calculate the ionic loss of the HEM samples. The intensity of such signals was compared with that of the aromatic signals corresponding to the polymer backbones, which were usually not affected by the alkaline treatment because of their high chemical stability.

Size exclusion chromatography (SEC)

SEC was used to determine the molecular weight and dipersity (*Đ*) of the non-cationic precursor polymers in Paper IV and V. A Malvern Viscotek instrument equipped with two PL-Gel Mix-B LS columns (2 × 30 cm) and OmniSEC triple detectors (refractive index, viscosity and light scattering). The analysis was carried

out using chloroform as eluent at a flow rate of 1 mL min^{-1} at 35 °C. A standard polystyrene (M_n = 96 kDa, $Đ$ = 1.03, Polymer Laboratories Ltd.) was used for calibration. Polymer samples were dissolved 24 h in advance and passed through a PTFE filter (pore size = 0.2 μm) before the analysis.

Intrinsic viscometry

Since the in-house SEC instruments use chloroform or tetrahydrofuran as eluent, and the polymers in Paper I-III were insoluble in both, the intrinsic viscosity ([η]) was measured. The [η] of a polymer gauges its ability to increase the viscosity of a solution and reflects the size of the polymer coil in dilute solution. This is related to the molecular weight of the polymer, temperature, and choice of solvent. For ionic polymers, the degree of ionization and charge density also matter. Usually, a suitable concentration of a salt in the polymer sample solution is necessary to prevent the polyelectrolyte effect, which results in the increase in the reduced viscosity with decreasing concentration. The widely accepted explanation is due to the increased molecular repulsion of the polymer upon dilution.[131]

The measurements were conducted using an Ubbelohde viscometer and 0.1 M LiBr in DMSO solution as blank at 25 °C, during which a constant temperature was ensured by applying a water bath. Polymer samples (in the Br^- form) were dried and precisely weighed before dissolution in the blank solution at an initial concentration around 1 g dl^{-1}. The efflux time of the polymer solution in the viscometer was recorded, and then the solution was diluted to several precise concentrations to record new times. Upon change of polymer samples and sample concentrations, 10-30 min was waited to equilibrate the temperature of the sample, and each measurement was repeated 4 times with high reproducibility. The [η] was calculated using:

$$\eta_{\mathrm{red}} = \frac{\frac{t_s}{t_b} - 1}{c} \quad (1),$$

$$\eta_{\mathrm{inh}} = \frac{\ln\left(\frac{t_s}{t_b}\right)}{c} \quad (2),$$

where t_b and t_s represent the efflux time of the blank and the sample solution at a concentration of c, respectively. The ratio t_s/t_b gives the relative viscosity (η_r), reflecting the increased viscosity of the solvent by the added polymer, derived under conditions where the density difference of the solvent and polymer solution is neglected for highly dilute solutions. The specific viscosity (η_{sp}) equals to $\eta_r - 1$. The reduced viscosity η_{red} is calculated as η_{sp}/c. η_{inh} is the inherent viscosity. Based upon Huggins'[132] and Kraemer's[133] equation, respectively, extrapolating η_{red} and η_{inh} to zero polymer concentration (c = 0), i.e., infinite dilution, gives the y-intercept which was taken as [η].

Differential scanning calorimetry (DSC)

DSC can be used to study the thermal transitions of a polymer sample. It reveals information about fundamental properties of the sample, e.g., the glass transition temperature (T_g), crystallization temperature, and melting temperature. The T_gs of precursor polymers in Paper IV and V were determined using a DSC Q2000 (TA instruments). The experiments were done by first heating to a predetermined temperature at a rate of 10 °C min^{-1} to remove any thermal history of the sample. After cooling to 25 °C, the sample was heated to the same temperature again at the same rate. The cationic polymers were not studied by DSC, mainly due to their limited thermal stability and the fact that their hydrophilic nature makes the complete removal of water in the samples difficult. The water acts as a plasticizer and largely affects the T_g. Cationic polymers are believed to have higher T_gs than corresponding non-ionic polymers, which is attributed to the presence of ions and the consequently strong electrostatic interactions between the polymer chains. As demonstrated by dynamic mechanical analysis, HEM polymers with a similar structure as in this thesis work showed T_gs above their decomposition temperatures.[134]

3.2.2 HEM characterizations

Thermogravimetric analysis (TGA)

The thermal decomposition of the dried cationic polymers in the Br^- form and the precursor polymers was studied using a TGA Q500 (TA instruments). Samples were first preheated to 150 °C for 20 min to eliminate any solvent residue, before cooling down and heating from 50 to 600 °C at a heating rate of 10 °C min^{-1}. The experiments were conducted in a heating chamber with N_2 flow. The weight change of the samples was recorded giving TGA traces, and the temperature at 5% weight loss was reported as the decomposition temperature ($T_{d,95}$).

Ion exchange capacity (IEC)

The IECs of HEMs in the Br^- form were determined by Mohr titrations. Around 0.03 g membrane pieces were thoroughly dried at 50 °C under vacuum during 48 h. After the precise weight was noted, the samples were transferred to bottles containing 25 mL 0.2 M aq. $NaNO_3$ and stored at room temperature for 48 h. During this time, the samples were fully immersed, and the bottles were carefully sealed to prevent water evaporation. The solutions were titrated in 4 portions (5 ml each) with 0.01 M aq. $AgNO_3$ using K_2CrO_4 as color indicator. The averaged endpoints of the titrations were used to calculate IEC_{Br} and IEC_{OH}.

Water uptake and swelling ratio

The water uptake of the HEMs was measured gravimetrically between 20 and 80 °C and was then calculated as:

$$WU = \frac{W_{\text{wet,OH}} - W_{\text{dry,OH}}}{W_{\text{dry,OH}}} \times 100\% \quad (3).$$

$W_{\text{wet, OH}}$ was the weight of the fully hydrated samples, which was measured after equilibration at each temperature. The samples were thoroughly dried and weighed in the Br^- form to avoid chemical degradation caused by OH^- ions at zero water content, and $W_{\text{dry, OH}}$ was calculated using $W_{\text{dry, Br}}$ and IEC_{Br} obtained by titration. After drying, the weight ($W_{\text{dry, Br}}$) and dimensions [length (l_{dry}) and thickness (t_{dry})] of the sample was precisely noted. Next, the samples were ion-exchanged to the OH^- form. After quick and repeated washing with DI water, the samples were equilibrated in DI water for 24 h at 20 °C, and 8 h at higher temperatures. Then the samples were quickly dried with tissue paper and weighed ($W_{\text{wet, OH}}$). Simultaneously, the length (l) and thickness (t) of the samples were measured, in order to calculate the in-plane and through-plane swelling (SW_{i} and SW_{th}), respectively. The swelling ratios were calculated as:

$$SW_{\text{i}} = \frac{l_{\text{wet}} - l_{\text{dry}}}{l_{\text{dry}}} \times 100\% \quad (4),$$

$$SW_{\text{th}} = \frac{t_{\text{wet}} - t_{\text{dry}}}{t_{\text{dry}}} \times 100\% \quad (5).$$

Morphology

The morphology of HEMs in the Br^- form was studied by small angle X-ray scattering (SAXS). SAXS is a non-destructive technique that probes the structure of a material with nanoscale resolution (1-100 nm). During the experiment, a collimated monochromatic X-ray beam illuminates the sample and a small portion

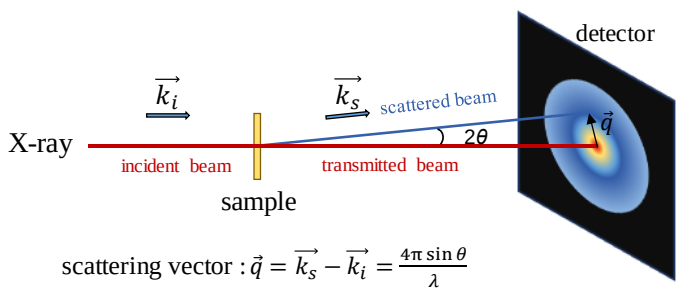

Figure 9. Schematic illustration of a SAXS experiment setup, created based on L.Barré.[135]

of the X-rays is scattered elastically in all directions by the oscillated electrons of the sample. The scattered beams retain the same energy and wavelength (λ) as the incident beam while having different scattering angles (2θ), and their intensity is recorded by a detector as a function of 2θ. The difference between the wave vectors k_i and k_s defines the scattering vector q, as shown in **Figure 9**.

The scattering curve is generated by plotting the intensity as a function of q. The nanostructure features in the sample scatter the X-rays at a certain angle, and the scattered beams at this angle would interfere constructively with each other, resulting in an increase of the intensity and an intensity maximum at q_{max}. The position of the maximum in the curve is correlated to the size of such feature, which is defined as the characteristic distance (d), and d can be calculated using q and Bragg's law as:

$$d = \frac{2\pi}{q_{max}} \quad (6).$$

The incompatibility of the hydrophobic backbone and the hydrophilic cations in an HEM is the basis for its micro-phase structure.[34] This feature can be detected by SAXS, and is revealed as an intensity maximum known as an 'ionomer peak' (**Figure 10**). The d value calculated using equation (6) indicates the distance between ionic clusters formed by ion aggregation.

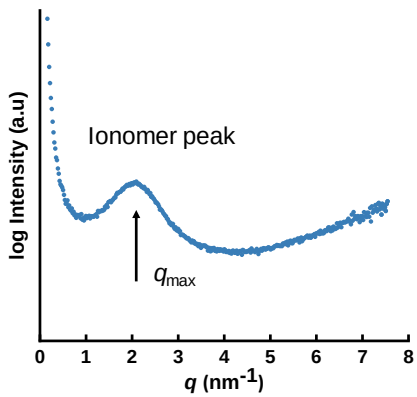

Figure 10. SAXS profile of an HEM based on QA functionalized PPO.

Samples were dried in advance, and the experiments were carried out on a SAXLAB instrument (JJ X-ray Systems ApS, Denmark) equipped with a Pilatus detector. Data was collected in the q-range 0.14-8.0 nm^{-1}.

Ion conductivity

The OH^- conductivity of the HEMs was measured by electrochemical impedance spectroscopy (EIS) while immersed in degassed deionized water between 20-80 °C.

The measurements were conducted on a Novocontrol high resolution dielectric analyser V 1.01 S at 50 or 10 mV between 10^7-10^0 Hz. The sample was quickly assembled into a 2-probe cell as shown in **Figure 11**. Two rectangular stainless steel electrodes were placed diagonally on two sides of the sample, to measure the in-plane membrane resistance (R) while avoiding surface conductivity. The compact assembly was placed in a Teflon holder, and degassed water was added to hydrate the sample. Then the cell was sealed with brass plates and plastic screws.

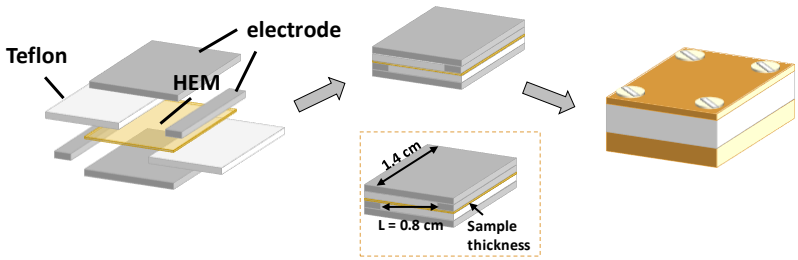

Figure 11. Sample cell configuration for EIS experiments.

For each HEM, at least two samples were measured. The conductivity (σ) was calculated by the instrument as:

$$\sigma = \frac{L}{A \times R} \qquad (7),$$

where L is the distance between the two rectangular electrodes, which is 0.8 cm while neglecting the sample thickness (50-80 μm). A is the right-angle cross-sectional area of the sample, determined using the sample thickness and side length (1.4 cm). The acquired conductivity data from the instrument was plotted as a function of frequency, and the plateau value was reported (**Figure 12**).

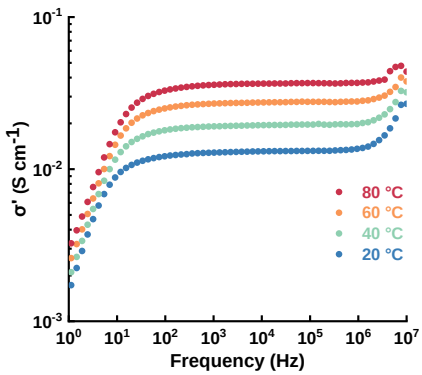

Figure 12. Conductivity data as a function of frequency measured between 20 and 80 °C. The plateau values were taken at around 10^4 Hz.

Chemical stability evaluations

The chemical stability of the HEMs was evaluated *ex-situ* by immersing samples in aq. NaOH solutions at elevated temperatures for predetermined time periods. After the treatment, samples were ion-exchanged to the Br^- form, dried and dissolved in DMSO-d_6 for ^1H NMR spectroscopy analysis. NMR analysis provides valuable information about the structural change of the samples, which is helpful to determine the degradation mechanism and calculate the degree of degradation, i.e., by ionic loss. Initially, aging of the samples was performed at 80 °C, since it is the prevailing operating temperature for many fuel cells and electrolyzer cells.[41, 136] To further accelerate the degradation reactions for ease of elucidating the active mechanisms, in many cases the temperature was raised to 90 °C. The molarity of the alkaline solutions also plays an important role in the degradation rate and mechanism. Throughout the thesis work it was varied from 1 to 10 M. During the alkaline stability evaluations, to prevent water evaporation, membrane samples were placed in a sealed pressure-resistant glass tube containing a Teflon insert, as shown in **Figure 13**.

Figure 13. Photo of containers used in alkaline stability evaluations placed inside an oven.

In paper II, the OH^- conductivity of some HEM samples was studied after treatment in 1 M NaOH at 80 °C during 7 days. EIS samples were stored as stated above, and the measurements were performed directly after quick washing of the degraded samples in DI water until neutral.

4 Summary of appended papers

This chapter summarizes the main findings of the synthesized HEMs *via* polyhydroxyalkylations included in this thesis work. The focus was placed on the rational molecular design of the polymer structures and important properties of the corresponding HEMs. More importantly, it was discussed how the polymer structures and cation arrangements affected the HEM properties.

4.1 HEMs carrying *N*-alicyclic cations (Paper I-III)

As presented in section 2.2.3, the DMP and ASU cations were very stable *N*-alicyclic QA cations toward OH^- attack. One way of incorporating them into polymers is *via* superacid-mediated polyhydroxyalkylation reactions using piperidones and arenes, followed by post-functionalization of the polymers. Such polymers are named poly(arylene piperidinium)s (PAPs), and their applications as HEMs were first demonstrated by Jannasch et al.[76, 96] The straightforward synthesis and remarkable HEM properties, especially the high alkaline stability, have boosted the development of HEMs based on PAPs. [38, 134, 137, 138] Even so, the DMP or ASU cations attached to PAPs appeared to be less stable and degraded faster than the small molecule cations in alkaline media. This is most likely due to the polymer backbone, whose rigidity impeded the relaxation of the cation ring and lowered the activation energy of the transition state of the degradation reactions.[76] Therefore, several strategies were developed in Paper I-III to construct polymers with different cationic arrangements, all with the aim to achieve a high alkaline stability of the cations and the HEMs.

4.1.1 Poly(fluorene alkylene)s (Paper I)

In Paper I, DMP and ASU cations were directly placed onto a rigid polymer backbone. The hypothesis was to fixate the cations and alleviate the distortion of the cation ring conformation, thereby preserving its high alkaline stability after being attached to the polymer. For this purpose, a fluorene unit was selected as the basis for the polymer structure. The C-9 position of fluorene is weakly acidic, making it possible to modify *via*, e.g., S_N2 alkylation reactions.

Polymer design and synthesis

Attaching the DMP or ASU cation at C-9 position of fluorene will arrange the cation in a more rigid position than it is in PAPs. This is because fluorene essentially is biphenyl with the two joint phenyl rings fused by a center five-membered ring, making it less flexible than biphenyl. To achieve this, a secondary piperidine was

introduced to the C-9 position of 2,7-diphenyl-9,9-*H*,*H*-fluorene (dPHF) and 9,9-*H*,*H*-fluorene (HF), respectively. The resulting compounds were denoted as dPFPip and FPip, respectively, and were later employed as aromatic monomers in polyhydroxyalkylations with either 1,1,1-trifluoroacetone (Ac) or 2,2,2-trifluoroacetophenone (Ap). During the polymerizations, the ketone monomers Ac and Ap were used in a molar excess of 1.2 eq. and 1.1 eq., respectively, to accelerate the polymerization and achieve sufficient molecular weight. dPFPip showed a much higher reactivity than FPip, giving film-forming polymers. Using the latter monomer only resulted in low-molecular-weight products. The two flanking phenyl rings of dPFPip not only facilitated the polymerization, but also enhanced the rigidity of the polymer backbone and the mechanical properties of the resulting polymer. Therefore, only precursor polymers based on dPFPip were functionalized with DMP or ASU cations by quaternization reactions (**Scheme 6**). The cations along with the central fluorene ring formed a spirocyclic or a bispirocyclic arrangement, respectively. In total, three polymers with structures presented in **Scheme 6** were cast into robust and flexible membranes from DMSO solutions, followed by ion-exchange to the Br^- form.

Scheme 6. Synthetic pathway toward the cationic polymers in Paper I.

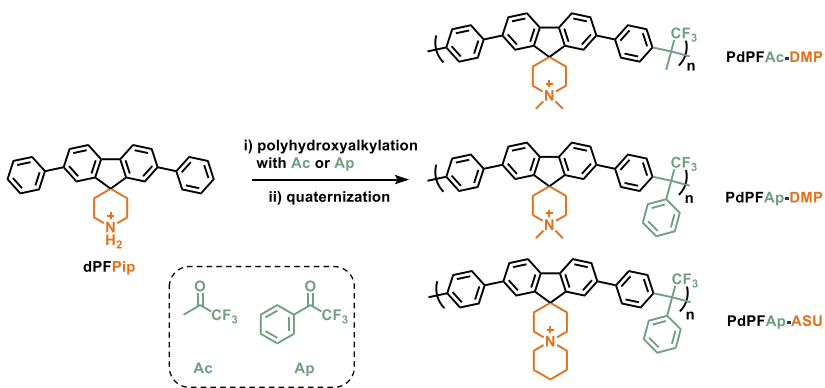

Characterizations

First, characterizations were carried out on membrane samples in the Br^- form, and the properties are listed in **Table 1**. IECs obtained from the Mohr titrations agreed well with the theoretical ones calculated from the polymer structures. Thermal stability evaluation by TGA revealed $T_{d,95}$ at the same level for the samples carrying the DMP cation, albeit the difference in polymer backbone (Ac and Ap). Enhanced thermal stability was observed for PdPFAp-ASU because of the ASU cation, most probably because of its bulky and rigid spirocyclic structure. This also contributed to the higher [η] of this sample compared to its counterpart PdPFAp-DMP prepared from the same precursor polymer.

Table 1. Properties of the poly(fluorene alkylene) membranes.

Sample	IEC[a] (meq.g^{-1})	$T_{d,95}$ (°C)	$[\eta]$[b] (dl g^{-1})
PdPFAc-DMP	1.83 (1.89)	237	0.78
PdPFAp-DMP	1.73 (1.70)	252	0.70
PdPFAp-ASU	1.60 (1.59)	330	0.95

[a] Values in the OH^- form determined by Mohr titrations and theoretical values in parentheses. [b] Measured in LiBr/DMSO solutions at 25 °C.

Next, HEMs were prepared by ion-exchange of the membranes in aq. NaOH, followed by characterization regarding water uptake and OH^- conductivity. Data collected at 80 °C are shown in **Figure 14a**. The water uptake and conductivity of the presented HEMs followed their IECs and temperature. For example, PdPFAp-ASU with the lowest IEC (1.61 meq.g^{-1}) showed a WU of 30-36% between 20-80 °C. Within this temperature range, the relatively low ionic content and water uptake resulted in limited OH^- conductivity of this HEM (14-36 mS cm^{-1}). As the IEC (and water uptake) increased, the conductivity was improved for the DMP-functionalized HEMs. For example, the conductivity of the latter exceeded 80 mS cm^{-1}, accompanied by 57% water uptake at 80 °C. This is rather high for an HEM based on random copolymer with an IEC below 2 meq.g^{-1}, in comparison with literature values.[53, 96, 139-141] Seemingly, among the three HEMs presented here, the IEC of PdPFAc-DMP (1.83 meq. g^{-1}) had reached a critical value to reach an efficient water uptake and ion transport. A further increase in IEC would be possible by preparing polymers using monomer FPip. For instance, a high IEC, up to 2.66 meq.g^{-1}, can be realized with a polymer based on FPip and Ac carrying the DMP cation. This will in principle greatly increase the water uptake and conductivity of the HEM. However, it requires a sufficiently high molecular weight of the precursor polymer to ensure mechanical strength of the HEM, which was found rather challenging to achieve.

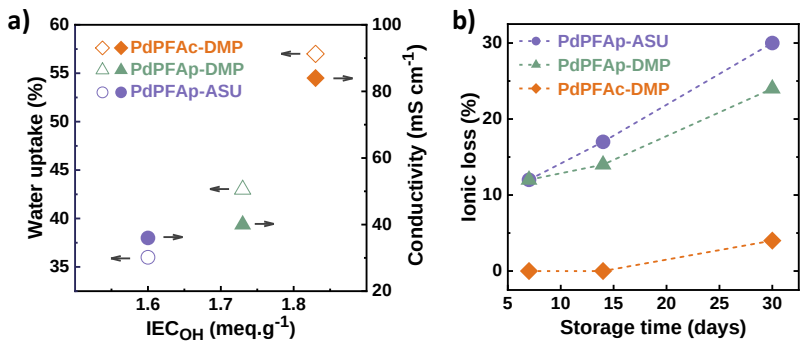

Figure 14. (a) Water uptake and OH^- conductivity of the HEMs at 80 °C as a function of IEC. (b) The ionic loss calculated for the HEMs after alkaline storage in 1 M aq. NaOH at 80 °C for 7, 14, and 30 days.

The alkaline stability of the HEMs was then studied by submerging samples in 1 M aq. NaOH at 80 °C for 7, 14, and 30 days. Afterwards, the chemical structure of the samples was assessed by ^{1}H NMR spectroscopy. The spectra after 30-day storage are shown in **Figure 15a-b**. Compared with the initial spectra (**Figure 15c-d)**, the aromatic signals between 7.0 and 8.5 ppm remained unchanged, indicating the high stability of the ether-free poly(fluorene alkylene) backbone. However, new proton signals appeared between 4.8 and 6.2 ppm, which were assigned to vinylic protons stemming from Hofmann elimination reactions of the DMP cation (**Figure 15a-b**). With the addition of trifluoroacetic acid (TFA) to the NMR samples, a singlet was found at 9.4 ppm, attributed to the protonated tertiary amine (*e*). Both PdPFAp-DMP and PdPFAc-DMP were found to have degraded *via* Hofmann elimination, although the latter was far less sensitive as the new proton signals were nearly negligible (**Figure 15b**). Moreover, an additional set of vinylic signals were observed for PdPFAp-ASU, as both rings of the ASU cation contain β protons that allow for the Hofmann eliminations.

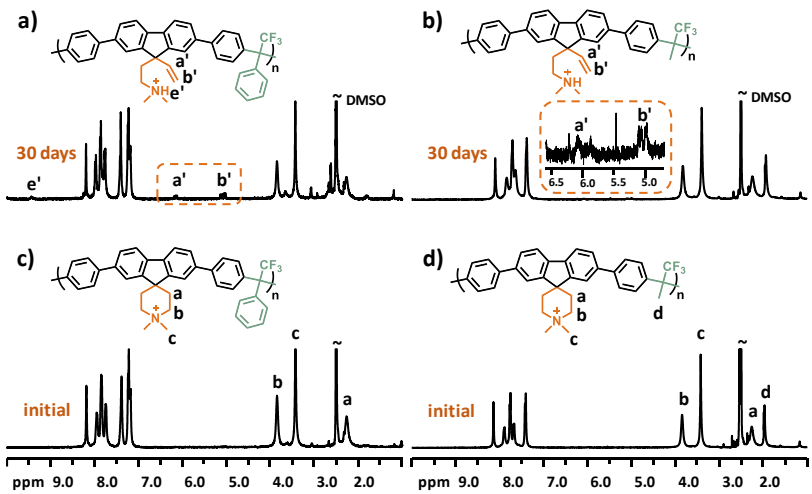

Figure 15. ^{1}H NMR spectra of (a-b) PdPFAp-DMP and (c-d) PdPFAc-DMP samples before and after storage in 1 M aq. NaOH at 80 °C during 30 days, recorded in DMSO-d_6 with TFA.

The degradation reactions led to loss of cations, which was calculated by comparing the integral of the new signals to the entire intact aromatic signals of the stable polymer backbone in the NMR spectra. The newly appeared amine signals above 9.0 ppm were used, and the ionic loss of the HEM samples was calculated and summarized in **Figure 14b**. PdPFAc-DMP was the most stable sample with 96% of its cations retained after 30 days. This was attributed to its slightly more flexible molecular structure and higher water uptake, compared to the other two HEMs. PdPFAp-ASU exhibited the highest ionic loss, which could be the consequence of

a lower cation flexibility imposed by the rigid backbone and the extra outer ring. In summary, it is clearly advisable to introduce high local cation flexibility, both regarding the backbone and the cation itself, and how the cation is attached to the polymer backbone, in order to achieve a high alkaline stability of the cation and the HEM.

4.1.2 Poly(biphenyl piperidine)s with side chains (Paper II)

Having gained experience from the work described in Paper I and information in literature, strategies of attaching the cations through flexible spacers were applied aiming for higher stability of the HEMs. Moreover, the use of spacers favors phase separation of the hydrophilic/hydrophobic domains in the HEM, which is beneficial for the ion transport.[142, 143] The piperidine ring of the precursor polymers in Paper I was a good grafting site due to the feasibility of *N*-alkylation reactions of the amine by alkyl halides. However, from a practical point of view, it was less ideal to use the existing homopolymers since the IEC values would be restricted. Also, it would be advantageous to avoid multi-step monomer synthesis. Therefore, in Paper II, commercially available compounds were used to prepare polymers *via* polyhydroxyalkylations. Copolymers with adjustable ionic compositions were synthesized and later grafted with cationic side chains.

Scheme 7. Synthetic routes toward cationic polymers in Paper II.

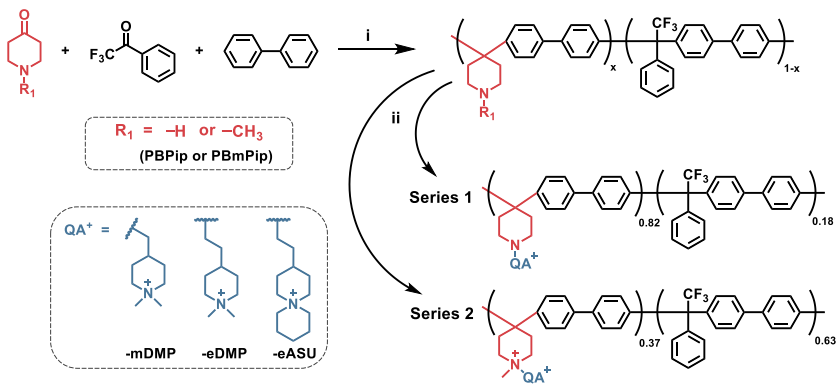

As shown in **Scheme 7**, two precursor poly(biphenyl piperidine)s, PBPip and PBmPip, were synthesized *via* superacid-mediated polyhydroxyalkylations. Meanwhile, three different bromoalkylated side chain compounds carrying DMP or ASU cations were designed, prepared, and employed for grafting of PBPip and PBmPip, yielding two series of cationic polymers. Notably, in Series 1, the backbone piperidine group remains neutral in alkaline media and functions as part of the spacer to the pendant cation, while in Series 2, the backbone piperidine group

was converted to a piperidinium cation after grafting and together with the pendant cation, formed a di-cationic configuration. The target IECs of the HEMs were between 2.00-2.24 meq g^{-1}, which was achieved by controlling the monomer feed ratio during the polymerizations and the resulting ionic/non-ionic composition of the precursor copolymers. PBPip contained 82% piperidine units while PBmPip had 37%.

The functionalization reactions were conducted using an excess of the grafting compounds and DIPEA as base. The progress of the reactions was monitored by extracting samples for ^{1}H NMR spectroscopy until full conversion. In principle, more than one alkyl halide compound can react with each secondary piperidine group in PBPip. However, due to the steric hindrance of the side chain compounds, no double substitution was observed, as evidenced by ^{1}H NMR spectroscopy and Mohr titrations. Experimental IECs were in good accordance with the theoretical ones (**Table 2**).

The thermal stability analysis on samples in the Br^- form revealed an overall higher $T_{d,95}$ for HEMs in Series 1 than those in Series 2 (**Table 2**). As expected, samples carrying the ASU cations were more thermally stable than their counterparts with DMP cations because of the bulkiness of the former cation. The [η] value of PBPip was slightly lower than for PBmPip, which may arise from the difference in the reactivity of the two piperidone monomers, as also observed during the polymerizations.

Table 2. Properties of the poly(biphenyl piperidine) membranes.

Series	Sample	IEC[a] (meq.g^{-1})	$T_{d,95}$ (°C)	[η][b] (dl g^{-1})
1	PBPip-mDMP	2.01 (1.96)	288	0.24
	PBPip-eDMP	2.04 (1.91)	289	
	PBPip-eASU	1.98 (1.77)	320	
2	PBmPip-mDMP	1.88 (1.88)	269	0.36
	PBmPip-eDMP	1.87 (1.85)	243	
	PBmPip-eASU	1.84 (1.79)	304	

[a] Values in the OH^- form determined by Mohr titrations and theoretical values in parentheses. [b] Measured in LiBr/DMSO solutions at 25 °C on the precursor polymers.

After ion-exchange, all the HEMs were transparent with good flexibility and toughness. Water uptake and conductivity of the HEMs at 80 °C are shown in **Figure 16**. The HEMs in Series 2 showed significantly lower and more controlled water uptake than their counterparts in Series 1, albeit the similar IECs (**Figure 16a**). This was most possibly attributed to the hydrophilic tertiary piperidine group

presented Series 1 HEMs which attracted more water. In addition, the recorded higher [η] of PBmPip than PBPip indicated a higher molecular weight, which may contribute to a higher degree of chain entanglement to restrain water uptake. Even so, the Series 2 HEMs overall reached a higher conductivity than Series 1 HEMs (**Figure 16b**). As clearly shown in **Figure 16c**, the HEMs in Series 2 were more efficient ion conductors as indicated by the nearly linear relationship and sharper trend observed for the conductivity values as a function of water uptake, which can be explained by more locally concentrated cations resulting from the copolymerization composition (37% for Series 2 *vs.* 82% for Series 1).

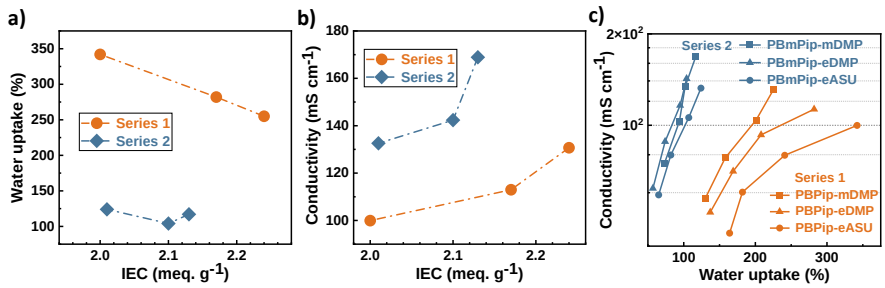

Figure 16. (a) Water uptake and (b) conductivity of the HEMs in Series 1 and 2 at 80 °C as a function of IEC. (c) Conductivity of the HEMs as a function of water uptake between 20 and 80 °C.

The possible chemical degradation reactions that can occur on the two Series of HEMs are different. For Series 1 HEMs, only the pendant cations are susceptible to OH^- attack and the backbone piperidine ring is alkali-stable. While in Series 2 HEMs, both the pendant and backbone cations are vulnerable. Using the cation structure of PBmPip-eASU as an example, **Figure 17a** shows possible degradation reactions, including Hofmann elimination at β-H (pathway 1, 5, and 6) and nucleophilic substitutions at α-Cs (pathway 2-4, and 7) of the DMP or ASU cations. In the case of HEMs in Series 1, only pathways 6 and 7 apply.

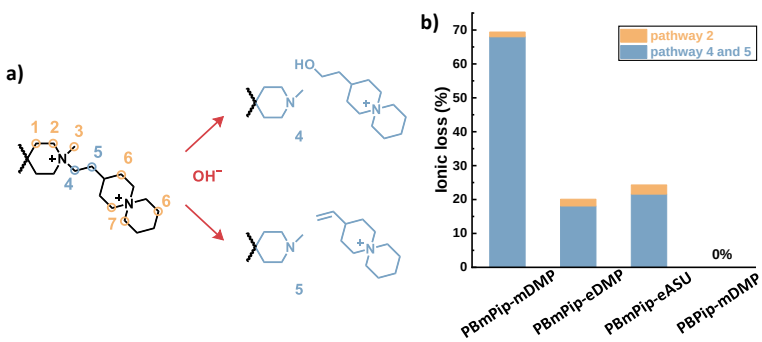

Figure 17. (a) Cationic arrangement of PBmPip-eASU with possible weak degradation points and two degradation pathways illustrated. (b) Ionic loss of the HEMs after storage in 1 M aq. NaOH at 80 °C for 30 days.

The alkaline stability of the HEMs was initially tested in 1 M aq. NaOH at 80 °C for 30 days. The results showed higher stability of HEMs in Series 1 than that of Series 2 (**Figure 17b**). After the storage, degradation *via* pathway 1, 4 and 5 was detected for the samples in Series 2, which resulted in 20-69% ionic loss. Specifically, pathways 4 and 5, i.e., scission of the spacer unit, accounted for 18-68% of the ionic loss. This was possibly caused by the strong electron-withdrawing effect of the pendant cations, hinting a more vulnerable cation arrangement in the samples in Series 2. Furthermore, the backbone cation is a sensitive target for OH^- attack, as explained by the ring distortion imposed by the rigid backbone to impair the chemical stability of the cation.[76] Under the same condition, samples in Series 1, devoid of backbone cations showed no distinct change in the ^1H NMR spectra. These samples were thus tested under a harsher condition, 2 M aq. NaOH at 90 °C for 30 days, and then showed only 6-8% ionic loss. Apparently, this is due to the presence of a more alkali-stable tertiary piperidine in the polymer backbone instead of an alkali-sensitive piperidinium cation. Moreover, the high water uptake of these AEMs played a role in ring relaxation, as well as hydrating the aggressive OH^- ions thus reducing its nucleophilicity.[86]

4.1.3 Improving HEM properties by monomer design (Paper III)

The previous study showed that replacing the backbone piperidinium with a tertiary piperidine greatly enhanced the alkaline stability of the HEMs. However, such tertiary piperidine led to excessive water uptake which compromised the mechanical strength of the HEMs. To replace piperidone as the ketone monomer, while retaining the merit of high alkaline stability of piperidinium cations, a trifluoromethylated piperidine monomer (TFPip) was designed. TFPip was employed in polyhydroxyalkylations with terphenyls (*p*T and *m*T), biphenyl (B), and dimethylfluorene (dF). Next, DMP or ASU cations were attached to the precursor polymers *via* quaternization reactions, generating in total 8 cationic polymers, as shown in **Scheme 8**.

Scheme 8. Synthetic pathways toward the cationic polymers in Paper III.

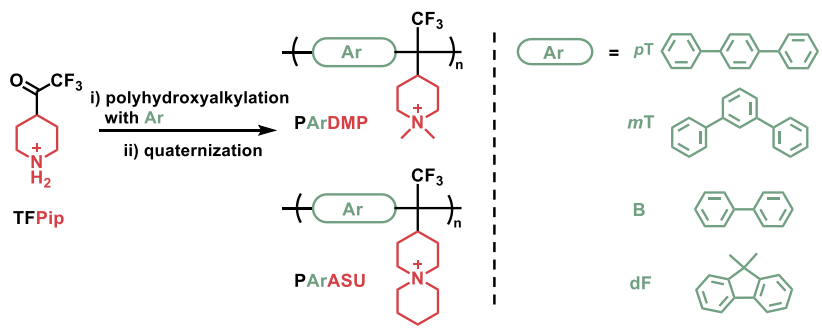

Polymerizations involving biphenyl or dimethylfluorene produced polymeric products with the expected chemical structures, as confirmed by ^{1}H NMR spectroscopy. However, casting films from polymer solutions in DMSO was not successful. The biphenyl-based film was free-standing yet rather brittle, and PdFPip was not film-forming. This indicated insufficient molecular weight of the two polymers. Several attempts to achieve high molecular weight products, e.g., by increasing the excess of TFPip (up to 40%) during the polymerizations in relation to the arenes, or adjusting the TFSA concentration, still failed to produce polymers with good film-forming properties. Still, the polymers were functionalized with DMP and ASU cations, respectively, and characterized with regards to the chemical structures and thermal properties ($T_{d,95}$ = 313-444 °C). Although the resulting polymers did not demonstrate practically useful HEMs, the rather high IEC values (2.25-2.75 meq.g^{-1}) made them potentially useful as ionomers for the catalyst layers.

Polymerizations of TFPip and terphenyls were successful, using 20% excess of TFPip. Robust and flexible films were obtained from both precursor polymers. This could be related to their more rigid polymer backbones compared to biphenyl and dimethylfluorene, and a relatively higher reactivity of *p*T and *m*T in the polymerizations to reach sufficient molecular weight. Furthermore, the polymerization using *p*T was selected for optimization due to the high reactivity, in order to reach a high molecular weight which is beneficial for HEM properties. By varying the excess of TFPip, TFSA amount and reaction time, different P*p*TPip samples and corresponding P*p*TDMP HEMs were prepared. The [η] value and water uptake of the HEMs were characterized, and the results are shown in **Table 3**. The highest [η] = 1.37 dl g^{-1} was achieved with 1 eq. *p*T, 1.4 eq. TFPip and 18 eq. TFSA during 576 h (entry 4). This sample also showed the highest OH^{-} conductivity at the lowest water uptake, demonstrating the importance of optimizing the polymerization conditions to prepare improved polymers and HEMs.

Table 3. Properties of P*p*TDMP HEMs derived from P*p*TPip samples prepared using different reaction conditions.

Entry	[η][a] dl g^{-1}	WU[b] (%)	σ[b] (mS cm^{-1})
1	0.52	174	167
2	0.83	128	155
3	0.78	121	156
4	1.37	104	178

[a] Measured on samples in the Br^{-} form in LiBr/DMSO solutions at 25 °C. [b] Measured on fully hydrated samples in the OH^{-} form at 80 °C.

Precursor polymers based on the terphenyls were functionalized with DMP and ASU cations, respectively, yielding 4 cationic polymers with IEC values between

2.07 and 2.23 meq g^{-1} (in the OH^- form). The thermal stability of the cationic polymers was surprisingly higher than the precursor polymers, which is in contrast with previous studies.[76, 101, 144] This can be ascribed to the fact that the precursor polymers were protonated and the presence of triflate ($TFSA^-$) as counter ions.

OH^- conductivities and water uptake of the optimized *p*T-based (**Table 3**, entry 4) and *m*T-based HEMs are shown in **Figure 18**. Remarkably, all the HEMs reached high OH^- conductivities, up to 178 mS cm^{-1} at 80 °C. Between 20 and 80 °C, P*m*TDMP and P*m*TASU exhibited higher water uptake than their *p*T-based counterparts despite having the same IECs. This was most possibly due to the more rigid polymer backbone of the latter samples provided by *p*T which restricted the water uptake. In addition, the difference in molecular weight, as indicated by [η] (0.25 *vs.* 1.37 dl g^{-1}, P*m*TDMP *vs.* P*p*TDMP), also had an impact on the water uptake of the corresponding HEMs. Although similar conductivities were reached, *p*T-based HEMs were evidently more effective ion conductors, as shown in **Figure 18b**. With an increase in hydration number, P*p*T HEMs showed a much more rapid increase in conductivity than the P*m*T HEMs. A clear dilution effect was observed for the *m*T-based HEMs, where the significant water uptake in the HEM diluted the charge carriers (ions), resulting in a restricted increase in the conductivity with the water uptake.

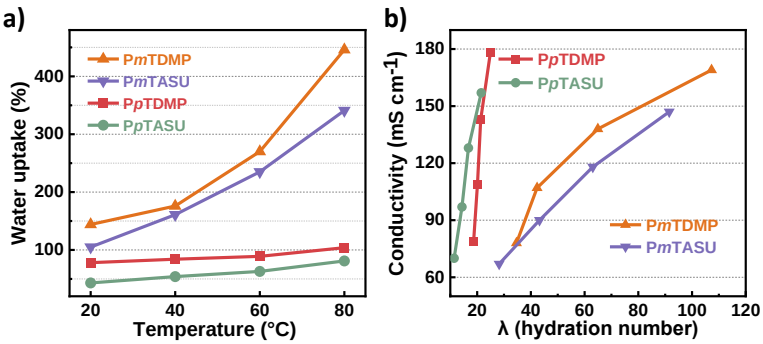

Figure 18. (a) Water uptake between 20 and 80 °C and (b) conductivity of the HEMs as a function of hydration number ($\lambda = n(H_2O)/(OH^-)$).

As before, the alkaline stability of the HEMs was evaluated. Samples were stored under various high-pH environments, from 2 M to 5 M aq. NaOH at 90 °C during 20 to 100 days. ^{1}H NMR spectra of the samples after treatment with 5 M aq. NaOH for 20 days were analyzed taking P*p*TDMP as an example (**Figure 19a**). P*p*TDMP mainly degraded *via* Hofmann elimination. Products from nucleophilic substitutions were detected too but were far less evident. The ionic loss after this treatment was benchmarked against HEMs based on PAPs (structures shown in **Figure 19b**). PTPipQ100 was chosen because of the pure *p*T backbone and PTPipQ83 was included due to its similar IEC and water uptake[145] as P*p*TDMP. The PAP HEMs

showed more pronounced structural changes in the ^{1}H NMR spectra with larger signals from degradation products than P*p*TDMP, indicating a higher alkaline stability of the latter. The ionic loss of the HEMs was calculated and is displayed in **Figure 19c**. PAP HEMs showed more than twice the ionic loss of P*p*TDMP after the same alkaline treatment. This confirmed the advantage of the cationic configuration of P*p*TDMP when it comes to improving the alkaline stability of the DMP cation, which was realized by using the TFPip monomer.

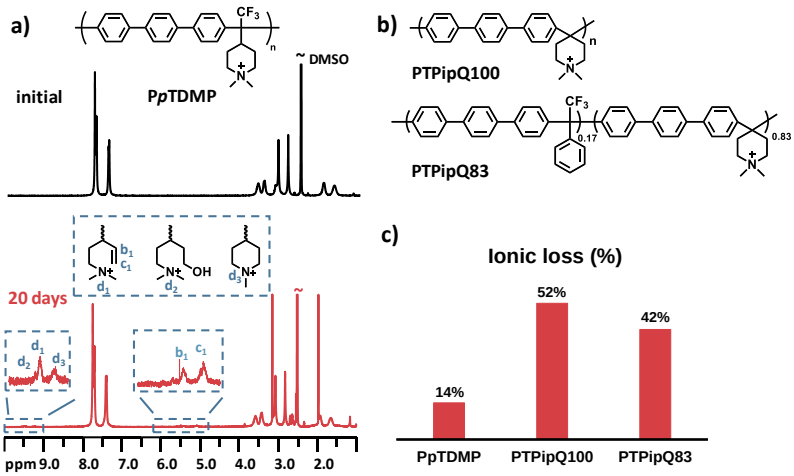

Figure 19. (a) ^{1}H NMR spectra of P*p*TDMP before and after treatment in 5 M aq. NaOH at 90 °C for 20 days. (b) Chemical structure of the reference PAP HEMs. (c) Ionic loss of the HEMs after storage under the aforementioned condition.

4.2 HEMs carrying QA cations on spacers (Paper IV-V)

Based on the experience from the work described in Paper I-III and literature, attaching cations away from the rigid backbone enhances ion mobility which favors efficient ion conduction and alkaline stability. Therefore, another two new ketone monomers were designed in the work of Paper IV-V and were subsequently employed in polyhydroxyalkylation reactions.

4.2.1 Poly(arylene alkylene)s (Paper IV)

As discussed in Paper III, the use of monomer TFPip to prepare HEMs resulted in significantly enhanced alkaline stability of the DMP cation and the corresponding HEMs. This was largely attributed to the more relaxed ring conformation of the DMP cation, due to the interstitial spacer units between the cation and the polymer backbone, as demonstrated in Paper II. This encouraged us to further increase the

local mobility of the cations by employing strategies to attach the cations to the polymer backbone *via* even longer spacers. In Paper IV, two ketone monomers TFAp-Pip and TFAp-Br were designed and synthesized (**Scheme 9**). Each monomer consisted of a trifluoromethyl ketone (or in a geminal diol form), which was essential for the sufficient reactivity in polyhydroxyalkylations. TFAp-Pip carries a secondary piperidine ring connected at the 4-position. As reported in literature,[129, 146] this attachment gives a high stability of the DMP cation than if it is attached at the 1(*N*)-position. TFAp-Br has a propyl chain with a terminal bromine atom which can be readily converted to QA groups by Menshutkin reactions with amines, as discussed in section 3.1.3.

Scheme 9. Synthetic routes and structures of cationic polymers in Paper IV.

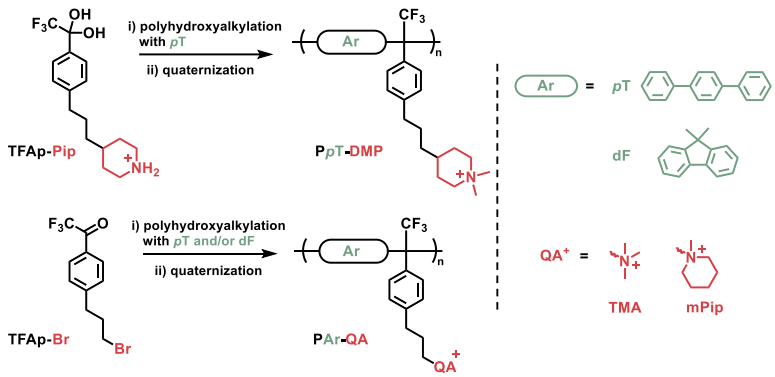

Polyhydroxyalkylation using TFAp-Pip and *p*-terphenyl resulted in a film-forming polymer, which was subsequently quaternized with MeI to give the cationic polymer P*p*T-DMP. The corresponding polymer carrying the ASU cation was not prepared for practical reasons due to its limited IEC. Attempts to polymerize TFAp-Pip and other aromatic monomers only resulted in low-molecular-weight products. On the other hand, TFAp-Br was readily polymerized with dimethylfluorene and/or *p*-terphenyl. With a 10% excess of TFAp-Br in relation to the arenes, three high molecular weight precursor polymers (PAr-Brs) were prepared (**Table 4**). Thermal stability analysis revealed a high $T_{d,95}$ (> 350 °C) for all the precursor polymers. DSC analysis was carried out on the PAr-Brs. For example, PdF-Br revealed a T_g value at around 240 °C. PAr-Brs were quaternized with trimethylamine to prepare the cationic PAr-TMAs. Additionally, P*p*T-Br was functionalized with mPip, to compare with P*p*T-DMP with regard to the different cationic arrangements of the piperidinium cation [attached to the 1(*N*)-position or the 4-position].

All the cationic polymers shown in **Scheme 9** were cast into mechanically strong HEMs. **Table 4** summarizes the properties of these samples. $T_{d,95}$ of the samples in the Br^- form fell into a narrow range between 225 and 248 °C. The water uptake and conductivity were measured on the samples in the OH^- form, and the data

followed the titrated IEC values and temperature. Among the five HEMs, PdF-TMA showed the best performance with a remarkably high conductivity, 175 mS cm^{-1} at 80 °C, attributed to its relatively high IEC and water uptake. Notably, the chemical structure of P*p*T-DMP and P*p*T-mPip were quite similar, but they reached rather different conductivity despite a similar IEC and water uptake. This indicated a possible difference in the nanostructure of the two samples. Although SAXS measurements showed indistinct ionomer peaks, atomic force microscopy of P*p*T-DMP revealed a clear phase separation feature of this sample.

Table 4. Properties of HEMs.

HEM	IEC_{OH}[a] (meq.g^{-1})	M_n[b] (kDa)	$T_{d,95}$ (°C)	WU[c] (%)	σ[c] (mS cm^{-1})
P*p*T-DMP	1.79	-	245	53	104
PdF-TMA	2.13	268	245	189	175
PdF-*p*T-TMA	2.05	153	242	113	152
P*p*T-TMA	2.00	131	225	71	131
P*p*T-mPip	1.84	131	248	52	81

[a] Values in the OH^- form determined by Mohr titrations. [b] Molecular weight of the corresponding precursor polymers acquired from size exclusion chromatography (SEC) analysis using chloroform as eluent. [c] Measured on HEMs in the fully hydrated state at 80 °C.

The main motivation behind the design of monomer TFAp-Pip was still to prepare HEMs with high alkaline stability. The alkaline stability of P*p*T-DMP was evaluated under different conditions in 2-10 M aq. NaOH at 90 °C for 10 and 20 days. The sample only showed signs of degradation detected by ^{1}H NMR spectroscopy after storage in 5 M alkali for 20 days. To better probe the active degradation mechanism, the spectrum after treatment in 10 M NaOH for 10 days is shown together with the initial spectrum in **Figure 20**. As expected, the samples underwent degradation *via* Hofmann elimination, as indicated by the rise of vinylic signals between 4.8-5.6 ppm and an amine signal at 9.3 ppm. Another amine signal was detected at 9.2 ppm, which could be ascribed to the tertiary piperidine resulting from nucleophilic substitution of the methyl group. Comparing the integrals of these amine signals to that of the entire aromatic region, the total ionic loss was calculated to be 56%. Under milder conditions at 5 M and 7 M during 10 days, the ionic loss was estimated to be less than 5 and 7%, respectively, making P*p*T-DMP the most alkali-stable HEM in this thesis work.

In addition, P*p*T-mPip and P*p*T-TMA were selected for chemical stability evaluations. Both samples were first treated in 2 M aq. NaOH at 90 °C for 20 days which gave 3-4% ionic loss. This already suggested a reduced stability of the two

samples in comparison with P*p*T-DMP, which showed no structure change after the same treatment. Furthermore, after immersing P*p*T-mPip in 5 M aq. NaOH for 20 days, it was no longer soluble in DMSO-d_6 for NMR analysis. This strongly indicated its lower stability in comparison with P*p*T-DMP, further emphasizing the benefit of attaching the DMP cations at the 4-position.

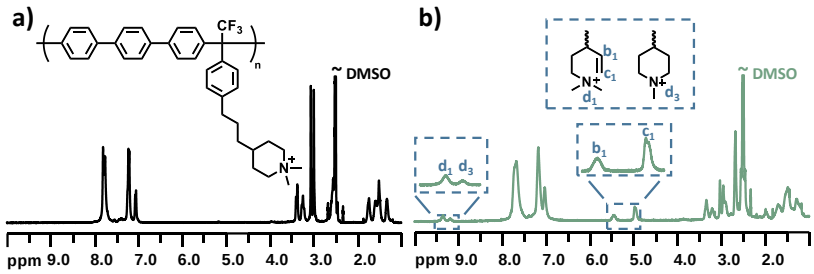

Figure 20. ^{1}H NMR spectra of P*p*T-DMP: (a) pristine and (b) after storage in 10 M aq. NaOH at 90 °C for 10 days, recorded in DMSO-d_6 with TFA.

4.2.2 Poly(xanthene)s (Paper V)

Monomer TFAp-Br presented in Paper IV was highly reactive in polyhydroxyalkylations with common aromatic monomers. Therefore, it was of great interest to further explore its use to synthesize additional polymers for HEM applications. Poly(xanthene) (PX) is a class of polymers based on xanthene unit, which has a tricyclic structure with two benzene rings fused by a pyran ring. This unique structure is the core of many widely used dyes such as fluorescein and rhodamines. Xanthene dyes can also be used as photoinitiators for radical polymerizations.[147] The first reported PX was prepared by Zolotukhin et al. using polyhydroxyalkylations involving 4,4'-biphenol and various trifluoromethylketones.[148] The polymers were well defined and of high molecular weight. PXs were not explored as HEM materials until very recently, when Zhang et al. reported the polymerization of 9,9-dimethylxanthene and isatin *via* a polyhydroxyalkylation.[149] The *N*-H site of the isatin moiety in the polymer was then grafted with TMA cations *via* sidechains. The resulting HEM of the highest IEC (2.1 meq.g^{-1}) reached a high OH^- conductivity, 205 mS cm^{-1} at 80 °C at a relatively low water uptake (62%) and swelling (< 15%). The good properties of the HEMs were attributed to the combination of a twisted backbone and flexible sidechains. The rigid backbone was reported to prohibit efficient packing of the polymer chains, creating sub-nanometer cavities and ionic channels that promoted efficient ion transport.[149] In paper V, a series of QA-decorated PXs were prepared and studied as HEMs. As shown in **Scheme 10**, a precursor PX was first synthesized from TFAp-Br and 4,4'-biphenol, and then quaternized by amines to yield three polymers carrying different QA cations.

Scheme 10. Synthetic route toward QA-functionalized poly(xanthene)s.

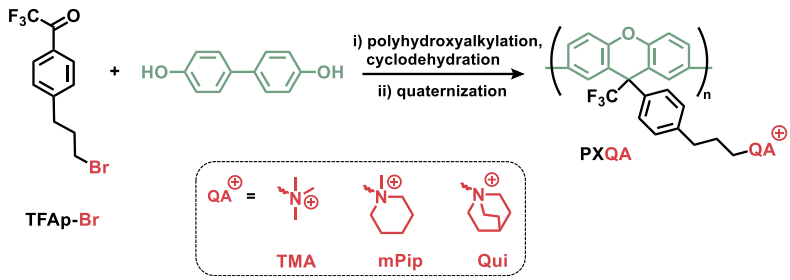

Initial trials of the polymerization involving TFAp-Br and 4,4'-biphenol revealed a high reactivity of both monomers. To achieve high molecular weight while avoiding gel formation, a stoichiometric feed of the two monomers was used and the polymerization was carried out at a low concentration. The polyhydroxyalkylation occurs at the *ortho*-position of the hydroxyl groups of the biphenol, which is the most activated, followed by a cyclodehydration of the adjacent -OH groups, forming the pyran ring. Complete cyclodehydration and absence of phenols in the polymer product (PX-Br) was confirmed by ^{1}H NMR spectroscopy. SEC revealed a high molecular weight (M_n > 100 kDa) for PX-Br, and transparent film could be obtained from a PX-Br solution in $CHCl_3$. DSC analysis of PX-Br revealed a T_g = 280 °C, higher than the equivalent polymer based on dimethylfluorene (PdF-Br, T_g = 240 °C). This demonstrates the higher rigidity of the poly(xanthene) backbone.

To demonstrate the use of PX for HEM application, PX-Br was functionalized with three amines, respectively, yielding cationic polymer PXTMA, PXmPip and PXQui, respectively (**Scheme 10**). HEMs were prepared from DMSO solutions of these cationic polymers, followed by ion exchange to the OH^- form. It is worth noting that reduced mechanical strength of the HEMs was observed in comparison to the PX-Br film. In fact, a very high molecular weight of PX-Br (M_n > 100 kDa) was essential to ensure sufficient robustness of the corresponding HEMs. Thermal decomposition of the HEM polymers in the Br^- form was studied by TGA, revealing $T_{d,95}$ values between 247 and 303 °C (**Table 5**). PXQui was the most thermally stable polymer owing to the cage-like structure of the quinuclidinium cation.

As expected, the water uptake and OH^- conductivity of the PX HEMs increased with increasing IEC and temperature between 20 and 80 °C. The results obtained at 80 °C are summarized in **Table 5**. The highest conductivity of 129 mS cm^{-1} was reached by PXTMA at a water uptake of 175% at 80 °C. This was relatively higher than most TMA-functionalized poly(arylene alkylene)s reported in the literature.[75, 77, 150, 151] However, PX-TMA did not outperform HEMs based on the same monomer TFAp-Br in Paper IV, although the IEC was slightly higher. The reason behind this is not very clear at this point. The difference of these HEMs lies not only in the backbone structure, but also in the molecular weight of the precursor polymers.

Overall, the molecular weight of the precursor polymers in Paper IV was much higher than that of PX-Br. This ensured better mechanical properties of the resulting HEMs, as also observed during the handling of the materials.

Table 5. Properties of PX-based HEMs.

HEM	IEC_{OH}[a] (meq.g^{-1})	WU[b] (%)	σ[b] (mS cm^{-1})	$T_{d,95}$ (°C)
PXTMA	2.27 (2.26)	175	129	247
PXmPip	2.05 (2.08)	149	114	268
PXQui	2.03 (2.03)	149	104	303

[a] Values in the OH^- form determined by Mohr titrations and theoretical values in parentheses. [b] Measured on HEMs in the fully hydrated state at 80 °C.

The alkaline stability of the PX HEMs was evaluated in 1 M or 2 M aq. NaOH at 80 or 90 °C for 720 h. After the treatments, samples were subjected to ^{1}H NMR analysis, as in previous studies. Particularly, to evaluate the alkaline resistance of the xanthene backbone, TGA was performed on the treated samples to complement NMR data. After storage in 1 M aq. NaOH at 80 °C, the HEMs did not show any structural change by ^{1}H NMR analysis. The ^{1}H NMR spectra of PXTMA and PXQui are given as examples (**Figure 21a** and **c**). The spectra after aging overlapped perfectly with the initial ones. In addition, the TGA trace of PXTMA after this treatment, shown in **Figure 21b**, coincided well with the initial trace, further confirming the absence of any structural change. Next, the samples were exposed to harsher conditions in 2 M aq. NaOH at 90 °C. This time, new ^{1}H signals arose in the spectra of PXTMA and PXmPip. **Figure 21a** shows such a spectrum of PXTMA with new signals indicated by arrows, corresponding to protons from degradation products, most probably from nucleophilic substitution to the methyl group of the TMA cation. The TGA study agreed with the NMR data of these two HEMs, as the magnitude of the first weight loss decreased, indicating loss of the QA cation during the alkaline treatment (**Figure 21b** for PXTMA). Using the NMR data, the integrals of the newly appeared signals were compared with those of the intact aromatic region, revealing 3 and 4% ionic loss for PXTMA and PXmPip, respectively. Remarkably, PXQui showed no ionic loss, not even under the harsher condition (**Figure 21c** and **d**).

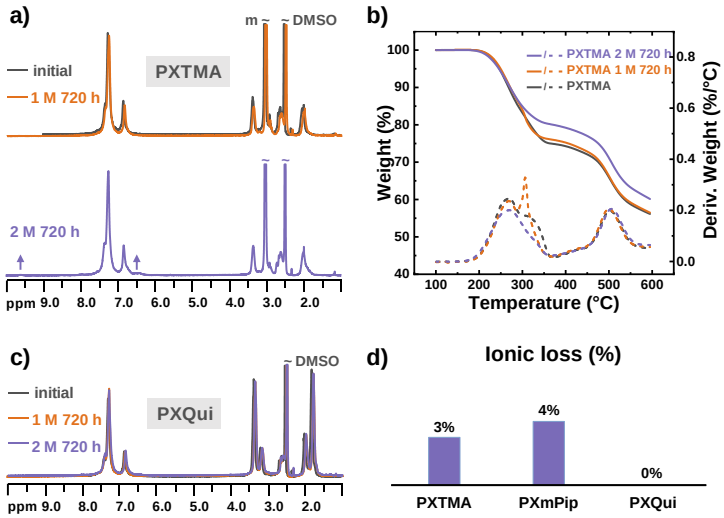

Figure 21. ^{1}H NMR spectra of (a) PXTMA, (b) PXmPip, and (c) PXQui before and after storage in aq. NaOH (1 M at 80 °C or 2 M at 90 °C) for 720 h, recorded in DMSO-d_6 with TFA. (d) Ionic loss of the samples after treatment under the latter (harsher) condition. The signal marked by '*m*' indicates the signal of the methyl groups of the TMA cation.

Most importantly, the xanthene backbone evidently remained unchanged as seen from the retained aromatic signals in NMR spectra and the onset of the second weight loss in TGA, which was correlated to the backbone decomposition. In addition, no sign of phenolic groups, which may potentially arise from hydrolysis of the aryl-ether bond, was detected by the NMR and TGA data. The combined results demonstrate the viability of PXs for HEM applications.

5 Conclusion and outlook

5.1 Conclusion

This thesis work explored superacid-mediated polyhydroxyalkylations to construct polymer backbones as starting points for polymer electrolytes applied in fuel cells and water electrolyzer cells. The polyhydroxyalkylation is a straightforward and efficient method to prepare high molecular weight polymers with well-defined structures. In a superacidic media, the reaction takes place between ketones and arenes, and is compatible with a wide range of different monomers. This allowed the synthesis of polymers, not only using commercially available monomers, but also using rationally designed new monomers to achieve the desired polymer structures. In total, 21 HEMs were synthesized and studied, including poly(fluorene alkylene)s (PFAs, Paper I), sidechain-grafted poly(biphenyl piperidine)s (PBPs, Paper II), poly(arylene alkylene piperidinium)s (PAAPs, Paper III), poly(arylene alkylene)s (PAAs, Paper IV), and poly(xanthene)s (PXs, Paper V). These materials were characterized with a focus on water uptake, ion conductivity, thermal stability, and alkaline resistance.

Paper I reports on the successful synthesis of three PFAs with spiro- and bis-spirocyclic cationic groups. Among the three samples, the one with the highest water uptake showed the highest OH^- conductivity and chemical resistance, which may be explained by its relatively higher IEC, slightly more flexible polymer backbone and cation arrangement. This inspired the study presented in Paper II, where the cation stability was further improved by attaching the cations *via* spacers. In addition, the OH^- conductivity was significantly increased by employment of a di-cationic arrangement which facilitated ion transport by constructing ionic channels. To achieve balanced properties with controlled water uptake, high conductivity and stability, new ketone monomers were designed for polyhydroxyalkylations. This was first successfully demonstrated by the work presented in Paper III, where the PAAPs outperformed the prevailing poly(arylene piperidinium)s in the literature with enhanced conductivity and stability. Another two new monomers were synthesized as described in Paper IV. With the cations linked to the polymer backbones *via* spacer units, the chemical stability of the HEMs was further improved. Lastly, PXs were presented as new HEM materials and showed a combination of excellent properties. More importantly, the ether-containing polymer backbone was found to be stable under the tested alkaline conditions.

5.2 Outlook

Although no *in-situ* evaluation and performance data are presented in this thesis work, selected HEMs are currently being evaluated in water electrolyzer cells and fuel cells. For future HEM development with national and international collaborators, there are several interesting points to consider:

1. Explore further use of PXs with different structures as HEMs, by employing monomers with varied structures.
2. Enhance mechanical properties by reinforcement using e.g., a porous polymer support layer to achieve high cell performance and durability.
3. Optimize polymerization reactions to prepare high-molecular-weight, narrow dispersity polymers to improve the mechanical strength of the membranes.
4. Reduce the HEM thickness to 5-30 μm, which is beneficial for the water management in fuel cells and prolonging lifetime of the device.
5. Place a focus on developing optimal ionomers for the alkaline devices, which together with the HEM significantly affect the performance and lifetime of the devices.

6 References

1. https://www.un.org/en/climatechange/what-is-climate-change).
2. J. P. Barton and D. G. Infield, *IEEE transactions on energy conversion*, 2004, **19**, 441-448.
3. M. Beaudin, H. Zareipour, A. Schellenberglabe and W. Rosehart, *Energy. Sustain. Dev.*, 2010, **14**, 302-314.
4. A. Hauer, J. Quinnell and E. Lävemann, in *Transition to Renewable Energy Systems*, 2013, pp. 555-577.
5. I. Staffell, D. Scamman, A. V. Abad, P. Balcombe, P. E. Dodds, et al., *Energy Environ. Sci*, 2019, **12**, 463-491.
6. C. Li and J.-B. Baek, *Nano Energy*, 2021, **87**, 106162.
7. H. A. Miller, *Curr. Opin. Electrochem.*, 2022, **36**, 101122.
8. B. Sundén, *The 4Ds of Energy Transition: Decarbonization, Decentralization, Decreasing Use and Digitalization*, 2022, 79-101.
9. O. Z. Sharaf and M. F. Orhan, *Renew. Sustain. Energy Rev.*, 2014, **32**, 810-853.
10. D. Akinyele, E. Olabode and A. Amole, *Inventions*, 2020, **5**, 42.
11. Y. Yang, C. R. Peltier, R. Zeng, R. Schimmenti, Q. Li, et al., *Chem Rev*, 2022, **122**, 6117-6321.
12. M. Mandal, *Chemelectrochem*, 2021, **8**, 36-45.
13. K.-D. Kreuer, *Chem. Mater.*, 2013, **26**, 361-380.
14. E. J. Park, C. G. Arges, H. Xu and Y. S. Kim, *ACS Energy Lett.*, 2022, **7**, 3447-3457.
15. Y. Wang, K. S. Chen, J. Mishler, S. C. Cho and X. C. Adroher, *Appl. Energy*, 2011, **88**, 981-1007.
16. B. Schwenzer, J. Zhang, S. Kim, L. Li, J. Liu, et al., *ChemSusChem*, 2011, **4**, 1388-1406.
17. S. Adhikari, M. K. Pagels, J. Y. Jeon and C. Bae, *Polymer*, 2020, **211**, 123080.
18. P. Millet, in *Compendium of Hydrogen Energy*, 2015, pp. 255-286.
19. N. Du, C. Roy, R. Peach, M. Turnbull, S. Thiele, et al., *Chem Rev*, 2022, **122**, 11830-11895.
20. L. J. Nuttall, A. P. Fickett and W. A. Titterington, in *Hydrogen Energy: Part A*, ed. T. N. Veziroğlu, Springer US, Boston, MA, 1975, pp. 441-455.
21. Y. Yang, P. Li, X. Zheng, W. Sun, S. X. Dou, et al., *Chem. Soc. Rev.*, 2022, **51**, 9620-9693.
22. R. A. Krivina, G. A. Lindquist, M. C. Yang, A. K. Cook, C. H. Hendon, et al., *ACS Appl. Mater. Interfaces*, 2022, **14**, 18261-18274.
23. U. Lucia, *Renew. Sustain. Energy Rev.*, 2014, **30**, 164-169.
24. O. Gröger, H. A. Gasteiger and J.-P. Suchsland, *J. Electrochem. Soc.*, 2015, **162**, A2605-A2622.
25. G. McLean, T. Niet, S. Prince-Richard and N. Djilali, *Int. J. Hydrogen Energy*, 2002, **27**, 507-526.
26. A. L. Dicks, *Curr. Opin. Solid State Mater. Sci.*, 2004, **8**, 379-383.
27. O. Yamamoto, *Electrochim. Acta*, 2000, **45**, 2423-2435.
28. K. A. Mauritz and R. B. Moore, *Chem. Rev.*, 2004, **104**, 4535-4586.

29. R. Yadav and P. S. Fedkiw, *J. Electrochem. Soc.*, 2012, **159**, B340-B346.
30. H.-Y. Jung and J. W. Kim, *Int. J. Hydrogen Energy*, 2012, **37**, 12580-12585.
31. R. S.-L. Yee, R. A. Rozendal, K. Zhang and B. P. Ladewig, *Chem. Eng. Res. Des.*, 2012, **90**, 950-959.
32. K. Jiao, J. Xuan, Q. Du, Z. Bao, B. Xie, et al., *Nature*, 2021, **595**, 361-369.
33. Z. Sun, B. Lin and F. Yan, *ChemSusChem*, 2018, **11**, 58-70.
34. J. R. Varcoe, P. Atanassov, D. R. Dekel, A. M. Herring, M. A. Hickner, et al., *Energy Environ. Sci*, 2014, **7**, 3135-3191.
35. L. Wang, M. Bellini, H. A. Miller and J. R. Varcoe, *J. Mater. Chem. A*, 2018, **6**, 15404-15412.
36. G. Huang, M. Mandal, X. Peng, A. C. Yang-Neyerlin, B. S. Pivovar, et al., *J. Electrochem. Soc.*, 2019, **166**, F637-F644.
37. H. G. Peng, Q. H. Li, M. X. Hu, L. Xiao, J. T. Lu, et al., *J.Power Sources*, 2018, **390**, 165-167.
38. J. H. Wang, Y. Zhao, B. P. Setzler, S. Rojas-Carbonell, C. Ben Yehuda, et al., *Nat. Energy*, 2019, **4**, 392-398.
39. T. Wang, L. Shi, J. H. Wang, Y. Zhao, B. P. Setzler, et al., *J. Electrochem. Soc.*, 2019, **166**, F3305-F3310.
40. N. Ul Hassan, M. Mandal, G. Huang, H. A. Firouzjaie, P. A. Kohl, et al., *Adv. Energy Mater.*, 2020, **10**, 2001986.
41. W. E. Mustain, M. Chatenet, M. Page and Y. S. Kim, *Energy Environ. Sci*, 2020, **13**, 2805-2838.
42. A. D. Mohanty, C. Y. Ryu, Y. S. Kim and C. Bae, *Macromolecules*, 2015, **48**, 7085-7095.
43. B. Zhang, Y. Hua and Z. Gao, *J.Power Sources*, 2022, **525**, 231141.
44. N. Agmon, *Chem. Phys. Lett.*, 1995, **244**, 456-462.
45. M. E. Tuckerman, D. Marx and M. Parrinello, *Nature*, 2002, **417**, 925-929.
46. D. Marx, A. Chandra and M. E. Tuckerman, *Chem. Rev.*, 2010, **110**, 2174-2216.
47. M. R. Hibbs, M. A. Hickner, T. M. Alam, S. K. McIntyre, C. H. Fujimoto, et al., *Chem. Mater.*, 2008, **20**, 2566-2573.
48. K. Kreuer, *J. Membr. Sci.*, 2001, **185**, 29-39.
49. J. Kizewski, N. Mudri, R. Zeng, S. Poynton, R. C. Slade, et al., *ECS Trans.*, 2010, **33**, 27.
50. N. Ziv and D. R. Dekel, *Electrochem. Commun.*, 2018, **88**, 109-113.
51. J. Y. Jeon, S. Park, J. Han, S. Maurya, A. D. Mohanty, et al., *Macromolecules*, 2019, **52**, 2139-2147.
52. N. Li, Y. Leng, M. A. Hickner and C. Y. Wang, *J. Am. Chem. Soc.*, 2013, **135**, 10124-10133.
53. S. Zhang, X. L. Zhu and C. H. Jin, *J. Mater. Chem. A*, 2019, **7**, 6883-6893.
54. N. Li, T. Yan, Z. Li, T. Thurn-Albrecht and W. H. Binder, *Energy Environ. Sci*, 2012, **5**, 7888-7892.
55. J. Zhang, K. Zhang, X. Liang, W. Yu, X. Ge, et al., *J. Mater. Chem. A*, 2021, **9**, 327-337.
56. W. W. Gou, W. T. Gao, X. L. Gao, Q. G. Zhang, A. M. Zhu, et al., *J. Membr. Sci.*, 2022, **645**, 120200.

57. H. S. Dang and P. Jannasch, *ACS Appl. Egergy Mater.*, 2018, **1**, 2222-2231.
58. L. J. Li, J. J. Zhang, T. Jiang, X. Q. Sun, Y. L. Li, et al., *ACS Appl. Egergy Mater.*, 2020, **3**, 6268-6279.
59. P. Zuo, Z. Xu, Q. Zhu, J. Ran, L. Ge, et al., *Adv. Funct. Mater.*, 2022, 2207366.
60. L. Wang, X. Peng, W. E. Mustain and J. R. Varcoe, *Energy Environ. Sci*, 2019, **12**, 1575-1579.
61. A. D. Mohanty, S. E. Tignor, J. A. Krause, Y.-K. Choe and C. Bae, *Macromolecules*, 2016, **49**, 3361-3372.
62. Y.-K. Choe, C. Fujimoto, K.-S. Lee, L. T. Dalton, K. Ayers, et al., *Chem. Mater.*, 2014, **26**, 5675-5682.
63. L. Zhu, X. D. Yu, X. Peng, T. J. Zimudzi, N. Saikia, et al., *Macromolecules*, 2019, **52**, 4030-4041.
64. L. Zhu, X. Peng, S. L. Shang, M. T. Kwasny, T. J. Zimudzi, et al., *Adv. Funct. Mater.*, 2019, **29**, 1902059.
65. L. Liu, Y. Deng, W. Zhang, J. Zhang, W. Ma, et al., *J. Membr. Sci.*, 2023, **672**, 121441.
66. R. Akiyama, N. Yokota and K. Miyatake, *Macromolecules*, 2019, **52**, 2131-2138.
67. E. J. Park, S. Maurya, M. R. Hibbs, C. H. Fujimoto, K. D. Kreuer, et al., *Macromolecules*, 2019, **52**, 5419-5428.
68. J. T. Fan, A. G. Wright, B. Britton, T. Weissbach, T. J. G. Skalski, et al., *ACS Macro Lett.*, 2017, **6**, 1089-1093.
69. J. Fan, S. Willdorf-Cohen, E. M. Schibli, Z. Paula, W. Li, et al., *Nat Commun*, 2019, **10**, 2306.
70. B. Xue, W. Cui, S. Zhou, Q. Zhang, J. Zheng, et al., *Macromolecules*, 2021, **54**, 2202-2212.
71. M. R. Hibbs, C. H. Fujimoto and C. J. Cornelius, *Macromolecules*, 2009, **42**, 8316-8321.
72. W. H. Lee, A. D. Mohanty and C. Bae, *ACS Macro Lett.*, 2015, **4**, 453-457.
73. T. H. Pham, J. S. Olsson and P. Jannasch, *J. Am. Chem. Soc.*, 2017, **139**, 2888-2891.
74. W. You, J. M. Ganley, B. G. Ernst, C. R. Peltier, H. Y. Ko, et al., *Chem Sci*, 2021, **12**, 3898-3910.
75. W. H. Lee, Y. S. Kim and C. Bae, *ACS Macro Lett.*, 2015, **4**, 814-818.
76. J. S. Olsson, T. H. Pham and P. Jannasch, *Adv. Funct. Mater.*, 2018, **28**, 1702758.
77. S. Maurya, S. Noh, I. Matanovic, E. J. Park, C. N. Villarrubia, et al., *Energy Environ. Sci*, 2018, **11**, 3283-3291.
78. M. S. Cha, J. E. Park, S. Kim, S.-H. Han, S.-H. Shin, et al., *Energy Environ. Sci*, 2020, **13**, 3633-3645.
79. W. You, K. M. Hugar and G. W. Coates, *Macromolecules*, 2018, **51**, 3212-3218.
80. K. M. Hugar, H. A. t. Kostalik and G. W. Coates, *J. Am. Chem. Soc.*, 2015, **137**, 8730-8737.
81. L. Liu, Q. Li, J. Dai, H. Wang, B. Jin, et al., *J. Membr. Sci.*, 2014, **453**, 52-60.
82. X. Lin, L. Wu, Y. Liu, A. L. Ong, S. D. Poynton, et al., *J.Power Sources*, 2012, **217**, 373-380.
83. K. J. Noonan, K. M. Hugar, H. A. Kostalik IV, E. B. Lobkovsky, H. D. Abruña, et al., *J. Am. Chem. Soc.*, 2012, **134**, 18161-18164.

84. N. Chen, Y. Jin, H. Liu, C. Hu, B. Wu, et al., *Angew. Chem., Int. Ed.*, 2021, **60**, 19272-19280.
85. A. D. Mohanty and C. Bae, *J. Mater. Chem. A*, 2014, **2**, 17314-17320.
86. M. G. Marino and K. D. Kreuer, *ChemSusChem*, 2015, **8**, 513-523.
87. T. Zhu, Y. Sha, H. A. Firouzjaie, X. Peng, Y. Cha, et al., *J. Am. Chem. Soc.*, 2020, **142**, 1083-1089.
88. Y. Zha, M. L. Disabb-Miller, Z. D. Johnson, M. A. Hickner and G. N. Tew, *J. Am. Chem. Soc.*, 2012, **134**, 4493-4496.
89. X. Liu, N. Xie, J. Xue, M. Li, C. Zheng, et al., *Nat. Energy*, 2022, **7**, 329-339.
90. J. D. Xue, J. F. Zhang, X. Liu, T. Huang, H. F. Jiang, et al., *Electrochem. Energy Rev.*, 2022, **5**, 348-400.
91. Z. W. Tao, C. Y. Wang, X. Y. Zhao, J. Li and M. D. Guiver, *Adv. Mater. Technol.*, 2021, **6**, 2001220.
92. D. R. Dekel, S. Willdorf, U. Ash, M. Amar, S. Pusara, et al., *J.Power Sources*, 2018, **375**, 351-360.
93. D. R. Dekel, M. Arnar, S. Willdorf, M. Kosa, S. Dhara, et al., *Chem. Mater.*, 2017, **29**, 4425-4431.
94. S. Willdorf-Cohen, A. Kaushansky, D. R. Dekel and C. E. Diesendruck, *J. Phys. Chem. Lett.*, 2022, **13**, 10216-10221.
95. N. Chen, Y. Jin, H. Liu, C. Hu, B. Wu, et al., *Angew. Chem.*, 2021, **133**, 19421-19429.
96. T. H. Pham, J. S. Olsson and P. Jannasch, *J. Mater. Chem. A*, 2018, **6**, 16537-16547.
97. N. J. Chen, C. R. Lu, Y. X. Li, C. Long and H. Zhu, *J. Membr. Sci.*, 2019, **572**, 246-254.
98. J. S. Olsson, T. H. Pham and P. Jannasch, *Macromolecules*, 2017, **50**, 2784-2793.
99. A. Serov, I. V. Zenyuk, C. G. Arges and M. Chatenet, *J.Power Sources*, 2018, **375**, 149-157.
100. X. Ge, F. Zhang, L. Wu, Z. Yang and T. Xu, *Macromolecules*, 2022, **55**, 3773-3787.
101. D. Pan, J. S. Olsson and P. Jannasch, *ACS Appl. Egergy Mater.*, 2022, **5**, 981-991.
102. D. R. Dekel, M. Amar, S. Willdorf, M. Kosa, S. Dhara, et al., *Chem. Mater.*, 2017, **29**, 4425-4431.
103. Y. Zhang, J. Parrondo, S. Sankarasubramanian and V. Ramani, *ChemSusChem*, 2017, **10**, 3056-3062.
104. S. Wierzbicki, J. C. Douglin, A. Kostuch, D. R. Dekel and K. Kruczala, *J Phys Chem Lett*, 2020, **11**, 7630-7636.
105. S. Wierzbicki, J. C. Douglin, R. K. Singh, D. R. Dekel and K. Kruczała, *ACS Catal.*, 2023, **13**, 2744-2750.
106. Z. Yang, J. Zhou, S. Wang, J. Hou, L. Wu, et al., *J. Mater. Chem. A*, 2015, **3**, 15015-15019.
107. L. Zhu, J. Pan, Y. Wang, J. Han, L. Zhuang, et al., *Macromolecules*, 2016, **49**, 815-824.
108. L. Tian, J. Li, Q. Liu, W. Ma, F. Wang, et al., *ACS Appl. Mater. Interfaces*, 2022, **14**, 39343-39353.
109. K. Min, J. E. Chae, Y. Lee, H.-J. Kim and T.-H. Kim, *J. Membr. Sci.*, 2022, **653**, 120487.

110. J. Miyake, T. Watanabe, H. Shintani, Y. Sugawara, M. Uchida, et al., *ACS Mater. Au*, 2021, **1**, 81-88.
111. H. H. Wang, C. Hu, J. H. Park, H. M. Kim, N. Y. Kang, et al., *J. Membr. Sci.*, 2022, **644**, 120160.
112. J. S. Olsson, T. H. Pham and P. Jannasch, *Macromolecules*, 2020, **53**, 4722-4732.
113. G. A. Olah, *Angew. Chem., Int. Ed.*, 1993, **32**, 767-788.
114. A. L. Rusanov, V. P. Chebotarev and S. S. Lovkov, *Usp. Khim.*, 2008, **77**, 578-584.
115. M. Gasonoo, A. Sumita, K. N. Boblak, K. Giuffre, T. Ohwada, et al., *J. Org. Chem.*, 2017, **82**, 6044-6053.
116. H. M. Colquhoun, M. G. Zolotukhin, L. M. Khalilov and U. M. Dzhemilev, *Macromolecules*, 2001, **34**, 1122-1124.
117. G. A. Olah, G. Rasul, C. York and G. S. Prakash, *J. Am. Chem. Soc.*, 1995, **117**, 11211-11214.
118. M. T. Guzmán-Gutiérrez, D. R. Nieto, S. Fomine, S. L. Morales, M. G. Zolotukhin, et al., *Macromolecules*, 2010, **44**, 194-202.
119. Y. Segawa, T. Higashihara and M. Ueda, *J. Am. Chem. Soc.*, 2010, **132**, 11000-11001.
120. M. Zolotukhin, S. Fomine, R. Salcedo and L. Khalilov, *Chem. Commun.*, 2004, 1030-1031.
121. A. M. Diaz, M. G. Zolotukhin, S. Fomine, R. Salcedo, O. Manero, et al., *Macromol. Rapid Commun.*, 2007, **28**, 183-187.
122. M. C. G. Hernandez, M. G. Zolotukhin, S. Fomine, G. Cedillo, S. L. Morales, et al., *Macromolecules*, 2010, **43**, 6968-6979.
123. L. I. Olvera, M. T. Guzmán-Gutiérrez, M. G. Zolotukhin, S. Fomine, J. Cárdenas, et al., *Macromolecules*, 2013, **46**, 7245-7256.
124. E. C. Mancilla, H. Hernández-Martínez, M. G. Zolotukhin, F. A. Ruiz-Treviño, M. O. González-Díaz, et al., *Ind. Eng. Chem. Res.*, 2019, **58**, 15280-15287.
125. L. I. Olvera, M. Rodriguez-Molina, F. A. Ruiz-Trevino, M. G. Zolotukhin, S. Fomine, et al., *Macromolecules*, 2017, **50**, 8480-8486.
126. A. R. Cruz, M. C. G. Hernandez, M. T. Guzmán-Gutiérrez, M. G. Zolotukhin, S. Fomine, et al., *Macromolecules*, 2012, **45**, 6774-6780.
127. U. J. Castillo, M. G. Zolotukhin, L. Fomina, D. R. Nieto, L. O. Garza, et al., *J. Mol. Model.*, 2013, **19**, 793-801.
128. M. J. O'Connor, K. N. Boblak, A. D. Spitzer, P. A. Gucciardo, A. M. Baumann, et al., *Tetrahedron Lett.*, 2010, **51**, 4984-4987.
129. A. Allushi, T. H. Pham, J. S. Olsson and P. Jannasch, *J. Mater. Chem. A*, 2019, **7**, 27164-27174.
130. C. Marestin, S. Chatti and R. Mercier, *Polymer*, 2021, **222**, 123647.
131. J. Eckelt, A. Knopf and B. A. Wolf, *Macromolecules*, 2008, **41**, 912-918.
132. M. L. Huggins, *J. Am. Chem. Soc.*, 1942, **64**, 2716-2718.
133. E. O. Kraemer, *Industrial & Engineering Chemistry*, 1938, **30**, 1200-1203.
134. N. Chen, H. H. Wang, S. P. Kim, H. M. Kim, W. H. Lee, et al., *Nat Commun*, 2021, **12**, 2367.
135. L. Barré, *X-ray and Neutron Techniques for Nanomaterials Characterization*, 2016, 665-716.

136. D. Li, A. R. Motz, C. Bae, C. Fujimoto, G. Yang, et al., *Energy Environ. Sci*, 2021, **14**, 3393-3419.
137. N. Chen, C. Hu, H. H. Wang, S. P. Kim, H. M. Kim, et al., *Angew. Chem., Int. Ed.*, 2021, **60**, 7710-7718.
138. X. Wu, N. Chen, H. A. Klok, Y. M. Lee and X. Hu, *Angew. Chem., Int. Ed.*, 2022, **61**, e202114892.
139. J. S. Olsson, T. H. Pham and P. Jannasch, *J. Membr. Sci.*, 2019, **578**, 183-195.
140. X. Li, K. Yang, Z. Li, J. Guo, J. Zheng, et al., *Int. J. Hydrogen Energy*, 2022, **47**, 15044-15055.
141. L. Zeng, W. Yuan, X. Ma, Q. He, L. Zhang, et al., *Macromolecules*, 2022, **55**, 4647-4655.
142. H. S. Dang and P. Jannasch, *J. Mater. Chem. A*, 2016, **4**, 17138-17153.
143. P. Jannasch and E. A. Weiber, *Macromol. Chem. Phys.*, 2016, **217**, 1108-1118.
144. D. Pan, T. H. Pham and P. Jannasch, *ACS Appl. Egergy Mater.*, 2021, **4**, 11652-11665.
145. T. Novalin, D. Pan, G. Lindbergh, C. Lagergren, P. Jannasch, et al., *J.Power Sources*, 2021, **507**, 230287.
146. T. H. Pham, A. Allushi, J. S. Olsson and P. Jannasch, *Polym. Chem.*, 2020, **11**, 6953-6963.
147. M. Encinas, A. Rufs, S. Bertolotti and C. Previtali, *Polymer*, 2009, **50**, 2762-2767.
148. L. I. Olvera, M. G. Zolotukhin, O. Hernandez-Cruz, S. Fomine, J. Cardenas, et al., *ACS Macro Lett.*, 2015, **4**, 492-494.
149. Q. Wang, L. Huang, Z. Wang, J. Zheng, Q. Zhang, et al., *Macromolecules*, 2022, **55**, 10713-10722.
150. W. H. Lee, E. J. Park, J. Han, D. W. Shin, Y. S. Kim, et al., *ACS Macro Lett.*, 2017, **6**, 566-570.
151. T. Jiang, C. Wu, Y. Zhou, S. Cheng, S. Yang, et al., *J. Membr. Sci.*, 2022, **647**, 120342.

Printed by Media-Tryck, Lund 2023 NORDIC SWAN ECOLABEL 3041 0903

LUND UNIVERSITY

Department of Chemistry
Faculty of Engineering

ISBN 978-91-7422-934-9